Contrib Mineral Petrol (2004) 148: 104–121
DOI 10.1007/s00410-004-0589-8

ORIGINAL PAPER

S. Jung · K. Mezger · S. Hoernes

Shear zone-related syenites in the Damara belt (Namibia): the role of crustal contamination and source composition

Received: 14 October 2003 / Accepted: 6 May 2004 / Published online: 10 August 2004

Abstract Geochemical and Nd-Sr-Pb-O isotope data for a suite of syn-collisional (ca. 520 Ma) syenites associated with a major shear zone in the Proterozoic Damara orogen (Namibia) constrain their sources and petrogenesis. Major rock types from within and outside the shear zone range from highly potassic nepheline syenites to quartz syenites and were primarily generated by fractional crystallization from a mantle-derived alkaline magma. Even the most primitive samples show pronounced depletion in Nb, Ti, Sr and P on a primitive mantle-normalized diagram, indicating the involvement of a recycled crustal component in the source. Extrapolation of the Sr-Nd-Pb-O isotope composition of the syenites from within the shear zone back to a hypothetical parental melt with 10 wt% MgO suggests derivation from a moderately enriched lithospheric upper mantle ($^{87}Sr/^{86}Sr$: 0.705, ϵ Nd: −2, $\delta^{18}O$: 6‰, $^{206}Pb/^{204}Pb$: 19.40, $^{207}Pb/^{204}Pb$: 15.82). More evolved quartz syenites show increasing $^{87}Sr/^{86}Sr$ ratios, increasing $\delta^{18}O$ values but less radiogenic ϵ Nd values and Pb isotopes with decreasing MgO, indicating assimilation of ca. 10% Archaean to Proterozoic local lower crust with unradiogenic ϵ Nd, high $^{87}Sr/^{86}Sr$ and low U/Pb. For samples from outside the shear zone a hypothetical parental melt with 10 wt% MgO has distinctly more radiogenic Sr but less radiogenic Nd isotopic composition ($^{87}Sr/^{86}Sr$: 0.712, ϵ Nd: −13), with strongly unradiogenic Pb isotope ratios ($^{206}Pb/^{204}Pb$: 17.40, $^{207}Pb/^{204}Pb$: 15.50), suggesting another strongly enriched lithospheric mantle source for these rocks. Differentiated syenites from outside the shear zone show decreasing $^{87}Sr/^{86}Sr$, increasing $\delta^{18}O$ values, more radiogenic ϵ Nd values and Pb isotope ratios with decreasing MgO indicating interaction with a lithospheric component with low Rb/Sr but high Sm/Nd and U/Pb.

S. Jung (✉)
Fachbereich Geowissenschaften,
Philipps-Universität Marburg,
Lahnberge/Hans-Meerwein-Straße, 35032 Marburg,
Germany
E-mail: jungs@staff.uni-marburg.de
Fax: +49-6421-2828919

S. Jung
Abt. Geochemie, Max-Planck-Institut für Chemie,
Postfach 3060, 55020 Mainz, Germany

K. Mezger
Institut für Mineralogie, Universität Münster,
Corrensstrasse 24, 48149 Münster, Germany

S. Hoernes
Mineralogisch-Petrologisches Institut der Universität Bonn,
Poppelsdorfer Schloß, 53115 Bonn, Germany

Introduction

Alkaline igneous rocks are volumetrically insignificant types (< 1% of all rock types worldwide) but they are widely distributed in space and time and occur in almost all tectonic settings except for mid-ocean ridges. Generally, they may be grouped into three categories: those formed in continental rift valleys or divergent continental margins, those formed in oceanic and continental intraplate setting without clear tectonic control, and those associated with subduction zone magmatism (e.g., Fitton and Upton 1987). Alkaline rocks in general can be derived from partial melting of metasomatized light rare earth elements (LREE) and large-ion-lithophile-elements (LILE) enriched upper mantle sources (Dawson 1987), from unmetasomatized asthenospheric mantle by very small degrees of partial melting followed by extensive crystal fractionation (e.g., Fitton 1987) or from interaction of asthenosphere-derived melts with the overlying lithosphere (e.g., Menzies 1987). Specific models for the generation of more evolved members of alkaline rock suites include crystal fractionation from alkali basaltic precursors combined with varying degrees of crustal contamination (Ewart 1982; Fitton 1987; Thirlwall and Burnard 1990; Fowler 1992; Foland et al. 1993; Brotzu et al. 1997; Smith et al. 1997; Mingram et al. 2000; Litvinovsky et al. 2002) or small-degree

partial melting of enriched upper mantle or even lower crust (Harris et al. 1983; Wooley and Jones 1987; Smith et al. 1988; Gleason et al. 1994; Zanvilevich et al. 1995).

Somewhat more sophisticated models have been suggested to explain the origin of syenites in particular. Syenites may form by melting of crustal rocks due to an influx of volatiles (Lubala et al. 1994), although this possibility seems to be quite rare. On the other hand, mafic syenites may originate by partial melting of metasomatized upper mantle (Sutcliff et al. 1990) whereas more evolved quartz syenites form by differentiation of an alkali basaltic magma (Brown and Becker 1986). Additionally, magma mixing processes with subsequent differentiation of the hybrid liquids can be important (Zhao et al. 1995; Litvinovsky et al. 2002). Lastly, mixing of mantle-derived, silica-undersaturated alkaline magmas with granitic magmas formed by melting of lower crustal material above a zone of mafic underplating is a viable process to explain the common coexistence of silica-undersaturated and oversaturated syenites.

The Proterozoic to Phanerozoic Damara orogen of Namibia contains pre-orogenic to syn-orogenic syenites in a number of localities. These include (from north to south and also from oldest to youngest) the (1) pre-orogenic Oas and Lofdal syenites, (2) the syn-orogenic Voetspoer syenite and (3) the syn-to late orogenic Otjimbingwe syenite. The last is clearly associated with a major shear zone, whereas the tectonic control for the Oas, Lofdal and Voetspoer syenites is unclear. Dating of movements along this shear zone may be achieved by dating minerals from synkinematic intrusions. Thus, dating primary magmatic minerals with a high closure temperature (e.g. zircon) from the syenites provide a powerful tool in determining the time of intrusion and, by implication, places constraints on the activation of a major mid-crustal shear zone.

One difficulty in evaluating models for the petrogenesis of the Damara syenites is the lack of data that place limits on the relative importance of source components (lower crust, upper crust, mantle) involved. Rare earth element (REE) abundances, whole rock Nd, Sr and O isotopes and Pb isotopes from leached feldspars are well suited for this purpose. Based on such a data set, this paper presents a detailed geochronological and isotopic study of the shear zone-hosted Otjimbingwe syenites. The results are used to constrain crystal fractionation processes and the effects of crustal contamination, and to infer the nature of the source and partial melting processes.

Analytical techniques

Whole rock powders were prepared using a jaw crusher, a ball mill and an agate mortar. Major and some trace elements (except for REE) were determined on fused lithium-tetraborate glass beads using standard XRF techniques. REEs were analyzed by inductively coupled plasma emission spectrometry following separation of the matrix elements by ion exchange (Heinrichs and Herrmann 1990). Loss on ignition (LOI) was determined gravimetrically after heating the samples at 1,050°C for 1 h (Lechler and Desilets 1987). FeO was measured titrimetrically with standard techniques. Accuracy and precision were controlled by repeated measurements against several international and in-house standards.

For the Rb-Sr and Sm-Nd whole rock isotope analyses the samples were spiked with a $^{149}Sm/^{150}Nd$ and a $^{85}Rb/^{84}Sr$ tracer and digested in concentrated HF-HNO_3 in 3-ml screw-top TEFLON vials inside Krogh-style TEFLON bombs at 200°C for 3 days. After complete dissolution the samples were dried and redissolved in 2.5 N HCl. Rubidium, Sr and REE were separated using standard cation exchange columns with a DOWEX AG 50 W-X 12 resin, using 2.5 N HCl for Rb and Sr and 6 N HCl for the REE. Neodymium and Sm were separated from the other REE on HDEHP coated TEFLON columns, using 0.12 N HCl for Nd and 0.3 N HCl for Sm. Isotope analyses were carried out at the Max-Planck-Institut für Chemie at Mainz with a Finnigan MAT 261 multicollector thermal ionization mass spectrometer operating in static mode. Rubidium, Sm and Nd were run on Re double filaments and Sr was run on W single filaments loaded with TaF_5. Neodymium isotopes were normalized to $^{146}Nd/^{144}Nd = 0.7219$. The total procedural blank for Nd was < 40 pg and is negligible. Repeated measurements of the La Jolla Nd standard gave $^{143}Nd/^{144}Nd = 0.511854 \pm 0.000031$ (2σ; $n = 24$). The reproducibility of the Sr standard (NBS 987) was $^{87}Sr/^{86}Sr = 0.710218 \pm 0.000029$ (2σ; $n = 24$) and the fractionation was corrected to $^{86}Sr/^{88}Sr = 0.1194$. Uncertainties in the $^{87}Sr/^{86}Sr$ and $^{143}Nd/^{144}Nd$ ratios are reported in the last two digits. Typical analytical errors in the $^{87}Rb/^{86}Sr$ and $^{147}Sm/^{144}Nd$ ratios are equal or better than 0.5 and 0.2%, respectively. For common Pb analyses, 30–50 mg of high-purity K-feldspar separates were washed in a mixture of 3:1 HCl:HNO_3 overnight on a hotplate to remove surface contamination and subsequently rinsed three times with ultra pure water. After this treatment, the separates were leached three times in a mixture of concentrated HF/HNO_3, which resulted in a weight loss of ~70–80%. Subsequently, the feldspars were dissolved in concentrated HF and, after evaporation, redissolved in 2.5 N HCl and 0.6 N HBr and loaded on TEFLON columns filled with DOWEX AG 1X8 anion exchange resin (100–200 mesh) in chloride form (Mattinson 1986). The Pb was extracted using conventional HBr/HCl techniques and was loaded on Re single filaments using the H_3PO_4–silica gel method (Cameron et al. 1969). Lead analyses were corrected for mass fractionation by a factor of 0.11% per a.m.u. The reproducibility of the standard NBS 982 was 0.068, 0.064 and 0.071% for the $^{206}Pb/^{204}Pb$, $^{207}Pb/^{204}Pb$ and $^{208}Pb/^{204}Pb$ ratio, respectively. The total procedure blank was < 100 pg Pb and is therefore negligible.

For U–Pb analyses of zircon, crushed rocks were passed through a 40–80 mesh sieve. Zircons were separated by magnetic separation, methylene iodide and

then handpicking to high purity. Only zircons free of inclusions were used and for each sample, 8–10 zircon grains were analyzed. The zircons were washed in warm deionized water to remove surface contamination and then spiked with a $^{205}Pb/^{233}U$ spike before digesting in concentrated HF/HNO_3 in 3-ml screw-top TEFLON vials inside Krogh-style TEFLON bombs at 200°C for several days. The Pb was separated using HCl–HBr and the U was separated using EICHROME resin and 2 N HNO_3/0.02 N HNO_3 chemistry. Lead isotope analyses were carried out as described above for common Pb. In order to correct for initial Pb composition, the Pb composition of leached K-feldspar from each sample was measured and taken as the initial Pb composition during zircon growth. Uncertainties for the U/Pb and Pb/Pb ratios, ages and corresponding uncertainties were calculated using the programs PBDAT and ISOPLOT (Ludwig 1991a, 1991b). Total blanks for U were < 30 pg and the U isotope analyses were corrected for 0.04% per a.m.u. based on repeat analyses of the NBS U 500 standard.

Oxygen isotope analyses were performed at the University of Bonn on ~10 mg aliquots of powdered whole-rock samples, using purified fluorine for oxygen extraction, followed by conversion to CO_2 (Clayton and Mayeda 1963). The $^{18}O/^{16}O$ measurements were made on a SIRA-9 triple-collector mass spectrometer manufactured by VG-Isogas. Analytical uncertainties are < 0.2‰.

Geological setting and rock types

The Damara orogen of Namibia comprises a deeply eroded section of a Pan-African mobile belt that can be divided into a north–south-trending coastal branch and a northeast–southwest-trending intracontinental branch (see inset to Fig. 1). This mobile belt consists mainly of 1.2–2.0 Ga-old basement gneisses, Pan-African (560–460 Ma-old) plutonic rocks and various metasedimentary rocks. The belt has been divided into several zones based mainly on stratigraphy, metamorphic grade, structure and geochronology (e.g., Miller 1983). Base-

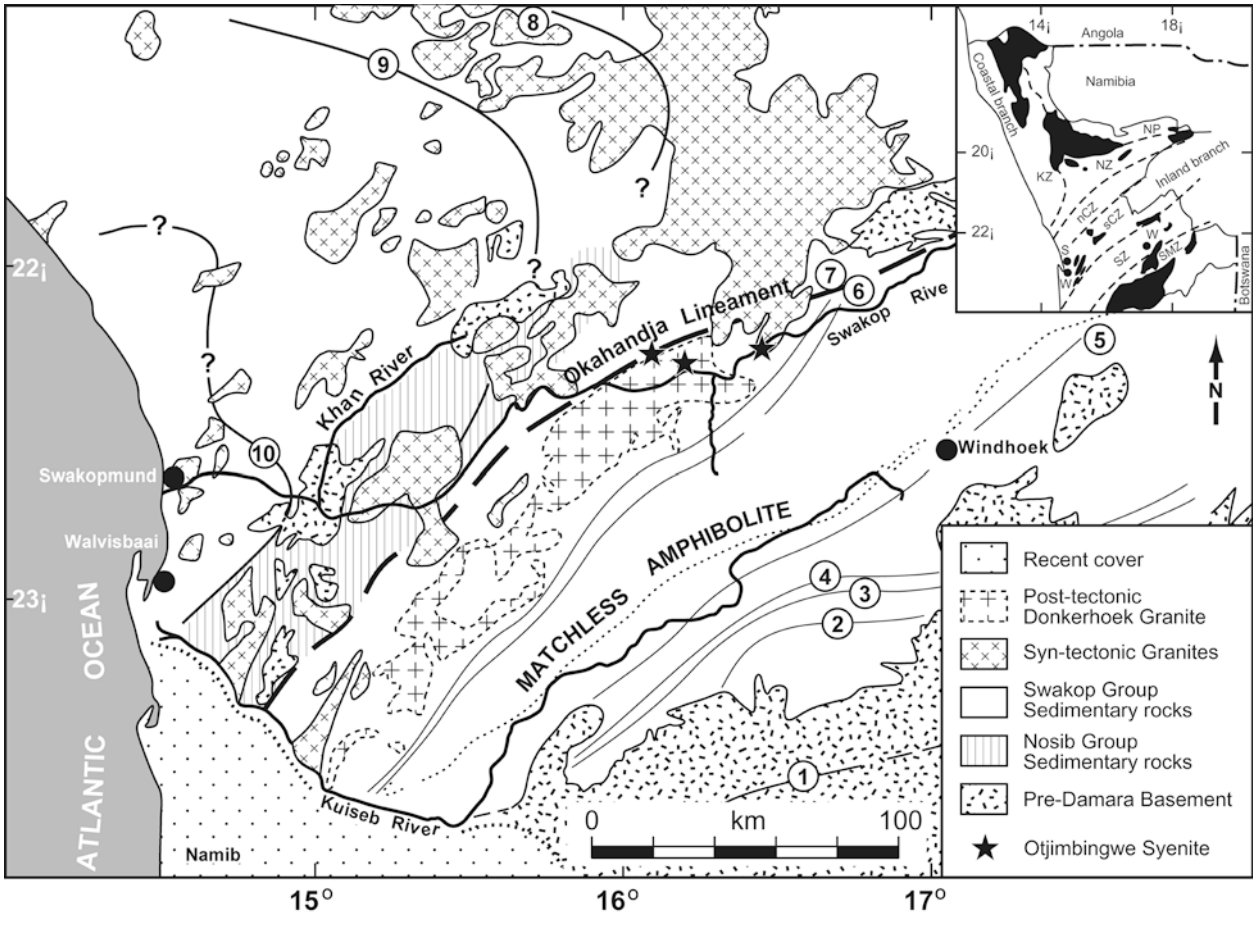

Fig. 1 Generalized geological map showing the study area within the Central Zone of the Damara orogen, Namibia. Abbreviations in inset: *KZ* Kaoko zone, *NP* northern platform, *NZ* northern zone, *nCZ* northern central zone, *sCZ* southern central zone, *SZ* southern zone, *SMZ* southern margin zone. Isograd map (Hartmann et al. 1983) gives the distribution of regional metamorphic isograds within the southern and central Damara orogen. Isograds: *1* biotite-in, *2* garnet-in, *3* staurolite-in, *4* kyanite-in, *5* cordierite-in, *6* andalusite <—> sillimanite, *7* sillimanite-in according to staurolite-breakdown, *8* partial melting due to: muscovite + plagioclase + quartz + H_2O <—> melt + sillimanite, *9* K-feldspar + cordierite-in, *10* partial melting due to: biotite + K-feldspar + plagioclase + quartz + cordierite <—> melt + garnet. *W* Walvisbay, *S* Swakopmund, *Wh* Windhoek

ment gneisses are overlain by Neoproterozoic (750 Ma-old) metasedimentary sequences, consisting of marble, calcsilicate rocks, quartzite, conglomerate, mica-schists, metamorphosed glaciogenic diamictites, banded iron-stone formations, Al-rich metapelites and migmatites. 560–460 Ma-old granites are the most common igneous rock type (ca. 94%) and crop out over an area of approximately 75.000 km^2. The remaining igneous bodies are equally divided between diorite and tonalite/granodiorite (Miller 1983).

In the Central Zone, the metamorphic grade increases from east to west reaching high-grade conditions with local partial melting in the coastal area (Hartmann et al. 1983). Here, low-pressure high-temperature granulite-facies conditions with temperatures between 680 and 750°C at 5–6 kbar were achieved (Masberg et al. 1992; Bühn et al. 1995; Jung et al. 1998a; Jung and Mezger 2003). The timing of orogenic events and the age of the peak of metamorphism within the Central Zone of the Damara orogen is now well constrained. Combined U/Pb monazite ages and Sm/Nd garnet-whole rock ages indicate that the time span of high grade metamorphism ranges from ca. 540 to 470 Ma, with ca. 510 Ma for the (main) peak of regional metamorphism (Jung and Mezger 2001, 2003).

In the Southern Zone, regional metamorphism is characterized by a Barrovian-type sequence with a general increase in the metamorphic grade from south to north (Fig. 1). The metamorphic grade reached up to 8 kbar at maximum temperatures of ca. 600°C. The age of this metamorphism is unconstrained, but Rb–Sr and K–Ar biotite ages indicate cooling to 300–350°C between 480 and 460 Ma (Miller 1983).

The Okahandja lineament, which can be traced several hundreds of kilometres from Namibia to Botswana, separates the Central Zone from the Southern Zone (Figs. 1 and 2). Miller (1983) suggested that the Okahandja lineament zone (OLZ) acted as a hinge for movements between the Central Zone and the Southern Zone. After the main peak of regional metamorphism in the Central Zone, this lineament zone was intruded by the late-orogenic Donkerhoek granite. It has been speculated that intrusion postdates the main deformation and peak of metamorphism in the Central Zone (Sawyer 1981); however, its intrusion is clearly synchronous with the final stages of significant tectonism in the OLZ. Due to intrusion of the Donkerhoek granite along it, most parts of the lineament are not preserved. The Proterozoic history of this lineament is a matter of debate; however, a tectonic regime of crustal extension during emplacement of the different igneous complexes (Otjimbingwe syenite and Donkerhoek granite) can be suggested (Miller 1983).

The Otjimbingwe syenite intruded within and outside the OLZ (Fig. 2). Syenites that crop out outside the shear zone (samples 98.1.15–98.1.19) intruded as metre-wide dykes into the Donkerhoek granite or into pelitic to semi-pelitic metasedimentary rocks of the Proterozoic Kuiseb Formation. Less common country rock types are intercalated impure calcite marbles and calc-silicate gneisses. All metasedimentary rocks display compositional layering on a centimetre to decimetre scale. The layering is discontinuous and boudinage is common. Leucocratic layers of tonalitic to granitic composition are common and are interpreted as small-scale intrusions from the nearby Donkerhoek granite. The other

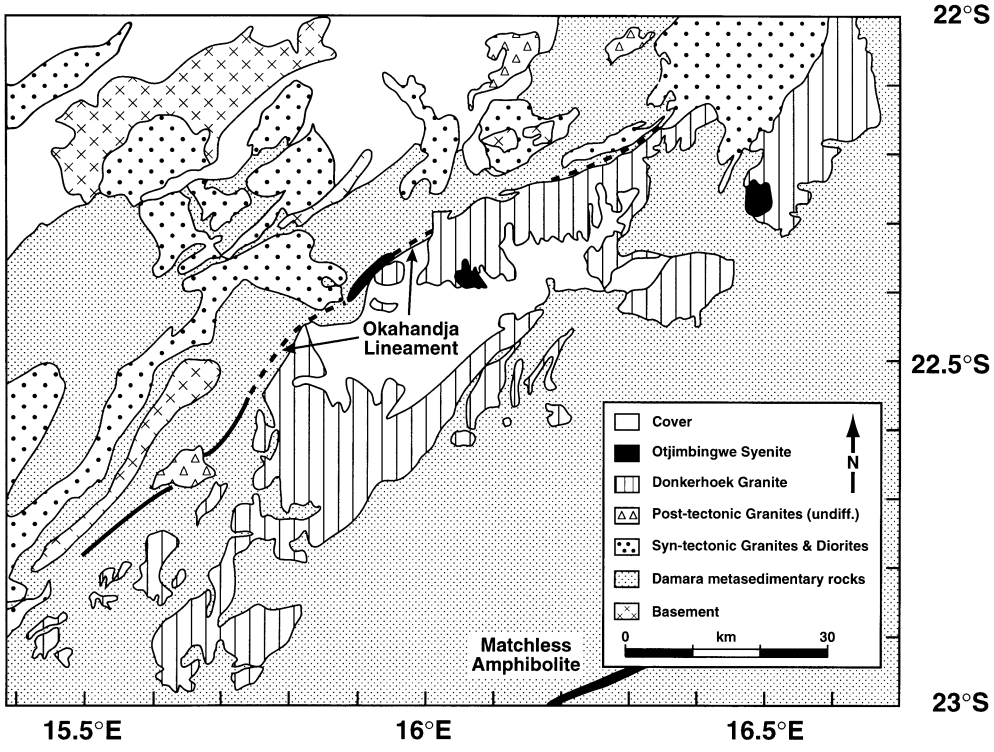

Fig. 2 Detailed map of the OLZ with syenite occurrences. Note the occurrence of the syenites within the shear zone close to pre-Pan African felsic basement, whereas the syenites from outside the shear zone are associated with granitic rocks of the Donkerhoek granite and metasedimentary rocks of the Kuiseb formation

syenite outcrops that are associated with the shear zone (samples M43–M54) are large, elongated, bodies. The main rock type of the Otjimbingwe syenite is a fresh, moderately foliated, dark-gray, porphyritic hornblende- and pyroxene-bearing massive syenite. Banding in some samples may resemble layering although it is suggested that these structures are in fact elongated lenses with contrasting proportions of mafic and felsic minerals. Deep crustal or country rock xenoliths are absent. Evidence of thermal effects in the contact zones has not been observed. A well-developed (F_1?) foliation, aligned parallel to the compositional layering, is defined by biotite in the pelitic country rock gneisses. In the syenite, remnants of an early phase of deformation are not preserved, but the second regional phase of deformation (D_2) produced a distinct fabric characterized by the orientation of K-feldspar and biotite in the syenite. This foliation (F_2) is parallel to the main regional schistosity (S_2) in the surrounding schists, leading to the suggestion that most of the complex is of pre- to syn-F_2 age. Mesoscopic shear-sense indicators e.g. rotated mafic xenoliths within the syenite are absent. Interpretation of microstructural features were used to infer that the F_2 deformation, which resulted in the development of the regional schistosity coincided with the inferred peak of metamorphism (Haack et al. 1980).

Petrography

Most syenites are texturally homogeneous and appear undeformed although some samples display a weak

Table 1 Selected mineral compositions from within shear zone syenites (Damara orogen, Namibia)

Sample	M52		M53		M46		M54		M51	
	Amph1	Amph2	Amph1	Amph2	Amph1	Amph2	Amph1	Amph2	Amph1	Amph2
SiO_2	49.95	49.56	46.63	48.61	48.71	50.16	48.45	47.59	54.36	52.07
TiO_2	0.55	0.56	0.78	0.62	0.57	0.37	0.71	0.92	0.02	0.14
Al_2O_3	4.26	4.28	6.58	5.85	5.27	4.26	5.10	6.27	1.20	2.56
FeO	14.56	14.82	16.24	15.30	14.82	14.17	16.18	16.32	13.18	15.55
MnO	0.34	0.34	0.42	0.31	0.37	0.29	0.33	0.45	0.37	0.40
MgO	14.53	14.36	12.69	13.39	13.71	14.57	13.26	12.61	15.50	14.00
CaO	11.17	11.31	11.02	11.35	11.27	11.43	11.00	11.38	12.03	11.23
Na_2O	1.74	1.64	1.90	1.64	1.71	1.50	1.76	1.57	0.45	0.84
K_2O	0.60	0.66	0.83	0.78	0.68	0.54	0.60	0.82	0.09	0.27
H_2O	2.00	2.00	2.00	2.00	2.00	2.00	2.00	2.00	2.00	2.00
Total	99.70	99.53	99.09	99.85	99.11	99.29	99.39	99.93	99.20	99.06

Sample	M52		M53		M46		M51		M43	
	Bt 1	Bt 2	Bt 1	Bt 2	Bt 1	Bt 2	Bt 1	Bt 2	Bt 1	Bt 2
SiO_2	38.85	38.60	38.31	38.92	38.85	38.34	37.61	37.35	36.28	36.93
TiO_2	1.49	1.81	2.29	2.07	2.20	2.03	2.24	2.13	2.48	2.54
Al_2O_3	12.64	12.04	12.44	12.48	12.24	12.40	13.08	13.11	13.17	12.91
FeO	16.42	16.71	17.90	17.48	17.64	17.67	20.53	20.87	21.83	21.75
MnO	0.23	0.20	0.23	0.28	0.27	0.19	0.19	0.20	0.27	0.21
MgO	16.16	15.64	14.23	14.32	14.51	14.79	12.05	12.18	11.43	11.23
CaO	0.00	0.00	0.00	0.00	0.00	0.00	0.02	0.02	0.00	0.01
Na_2O	0.06	0.06	0.10	0.13	0.10	0.04	0.12	0.07	0.06	0.04
K_2O	9.70	10.29	9.82	9.81	9.74	9.86	10.03	9.89	9.84	9.79
BaO	0.17	0.04	0.15	0.00	0.15	0.00	0.00	0.03	0.00	0.00
H_2O	4.00	4.00	4.00	4.00	4.00	4.00	4.00	4.00	4.00	4.00
Total	99.72	99.39	99.47	99.49	99.70	99.32	99.87	99.85	99.36	99.41

Sample	M46		M51		M43		M52		M53Plag	M46		M54Plag	M51Plag	M43Plag
	Cpx 1	Cpx 2	Cpx 1	Cpx 2	Cpx 1	Cpx 2	Plag	Akf		Plag	Akf			
SiO_2	52.86	52.94	51.63	51.93	52.08	51.72	66.71	63.47	68.39	68.90	64.81	66.26	67.32	67.60
TiO_2	0.05	0.10	0.13	0.17	0.11	0.11	0.00	0.00	0.00	0.00	0.00	0.00	0.00	0.00
Al_2O_3	0.67	0.64	1.28	1.64	0.75	1.04	19.98	18.26	19.27	18.86	18.05	20.06	19.99	19.52
FeO	10.08	9.93	11.14	11.33	11.70	12.21	0.00	0.00	0.00	0.00	0.00	0.00	0.00	0.00
MnO	0.40	0.39	0.34	0.31	0.42	0.46	0.00	0.00	0.00	0.00	0.00	0.00	0.00	0.00
MgO	12.05	12.31	11.03	10.86	11.17	11.31	0.00	0.00	0.00	0.00	0.00	0.00	0.00	0.00
CaO	22.64	22.65	22.52	22.25	23.00	22.77	0.97	0.00	0.27	0.25	0.00	2.20	0.58	0.63
Na_2O	1.04	0.87	1.04	1.11	0.72	0.76	11.06	0.67	11.32	11.41	2.12	9.37	11.30	11.33
K_2O	0.01	0.00	0.00	0.00	0.00	0.10	0.18	16.10	0.18	0.20	13.78	1.44	0.18	0.15
Total	99.80	99.83	99.11	99.60	99.95	100.48	98.90	98.50	99.43	99.62	98.76	99.33	99.37	99.23

foliation or banding. All samples show 120° grain boundaries between like minerals, indicating a substantial period of high-temperature static annealing after intrusion. The most mafic samples are medium to coarse grained and contain large euhedral perthitic alkali feldspar (Ab 6-12, An 1-2, Or 94-88, Table 1) and glomerophyric aggregates of clinopyroxene (augite to ferroan augite according to Deer et al. 1992), amphibole (magnesio-hornblende according to Deer et al. 1992), minor plagioclase (Ab 90-92, An 8-9, Or 1) and interstitial quartz. K-feldspar displays a concentric zoning of Ab-rich and Or-rich compositions. Large grains may show Carlsbad twinning and in some samples, K-feldspar shows concentric arrangement of small grains of clinopyroxene and apatite. Subhedral, locally corroded, green clinopyroxene is usually surrounded by late-stage amphibole and biotite (phlogopite–annite solid solution). In the more evolved samples, clinopyroxene is absent and subhedral green amphibole dominates over large flakes of dark brown biotite. Late-stage albite (Ab 97-98, An 1-2, Or 1) is common in these rocks. Clinopyroxene, amphibole, biotite and plagioclase are unzoned (Table 1). Accessory minerals include euhedral titanite, apatite, titanomagnetite, and zircon in decreasing order of abundance.

Geochronology

The geochronological results are reported in Table 2. Zircon was recovered from samples from within and outside the shear zone. The zircon population consists of euhedral pinkish to translucent grains. The zircons are 200–300 μm long with a length/width ratio of 3–5, indicating a magmatic origin for these grains (Pupin 1980). All selected zircon fractions were free of visible inclusions. Although no cores were determined optically, several fractions were abraded using an air abrasion chamber in order to check for older U–Pb age information within the inner crystal zones, or to eliminate the outer zones where recent Pb loss might have occurred. The six zircon fractions analyzed by conventional U–Pb techniques show an alignment generating a discordia that probably reflects a simple Pb loss history, with an upper concordia intercept age of 519.6 ± 8.5 Ma (Table 2; Fig. 3). The degree of discordance of air-abraded grains is not significantly different from that of untreated grains, supporting a simple Pb loss history for the zircons. In view of the inferred magmatic origin of the euhedral zircons the upper intercept age is interpreted as the time of the emplacement of the syenites. This age is similar to a Rb–Sr hornblende-whole rock age of 526 ± 7 Ma (Haack et al. 1988), but appears to be younger than the eight-point Rb-Sr whole rock isochron of 570 ± 41 Ma presented by Haack et al. (1988).

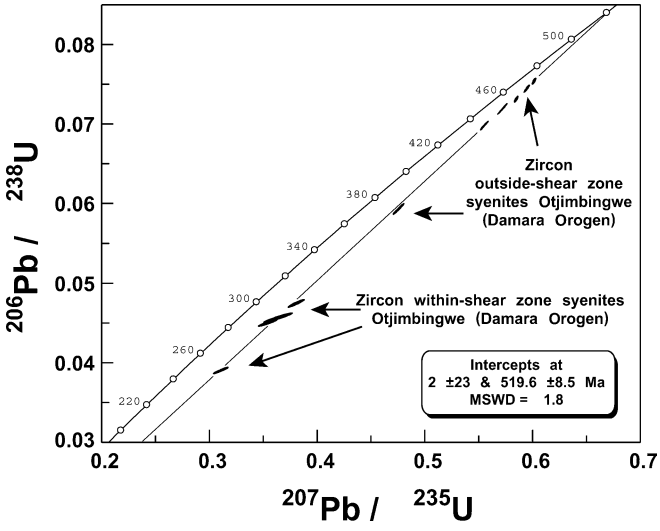

Fig. 3 U/Pb concordia diagram showing zircon analyses from syenites (Otjimbingwe, Damara orogen, Namibia)

Table 2 U–Pb zircon data from within shear zone syenites (M54) and outside shear zone syenites (98.1.17; 98.1.19) from the Damara orogen (Namibia)

Sample	98.1.17			98.1.19			M54			
	1	2	3	1	2	3	1	2	3	4
U (ppm)	4,401	4,806	2,639	1,488	2,586	3,687	12,399	14,370	14,175	13,885
Pb (ppm)	352	309	196	123	199	295	613	656	732	684
$^{206}Pb/^{204}Pb$	2,174	874	918	872	994	1,257	1,155	1,196	835	1,105
$^{208}Pb/^{206}Pb$	0.17554	0.10983	0.09847	0.13035	0.10906	0.12969	0.20461	0.18810	0.28780	0.19590
$^{207}Pb/^{206}Pb$	0.057819	0.057727	0.057680	0.057670	0.057682	0.057750	0.057819	0.057791	0.058170	0.057101
Error	0.000039	0.000094	0.000042	0.000044	0.000049	0.000049	0.000064	0.000046	0.000033	0.000720
$^{207}Pb/^{235}U$	0.58434	0.47407	0.55540	0.60073	0.57187	0.59406	0.36396	0.32063	0.38064	0.35413
Error	0.00115	0.00349	0.00260	0.00118	0.00317	0.00178	0.00900	0.00725	0.00525	0.00587
$^{206}Pb/^{238}U$	0.07330	0.05956	0.06984	0.07555	0.07191	0.07461	0.04565	0.03902	0.04746	0.04498
Error	0.00026	0.00046	0.00038	0.00026	0.00045	0.00031	0.00039	0.00040	0.00032	0.00028
$^{206}Pb/^{238}U$ age (m.y.)	456	373	435	469	448	464	288	247	299	284
$^{207}Pb/^{235}U$ age (m.y.)	467	394	449	478	459	473	315	282	328	308
$^{207}Pb/^{206}Pb$ age (m.y.)	523	519	518	517	518	520	523	522	536	495

Geochemistry

Major and trace elements

Major and trace element compositions are given in Table 3. In the syenites, SiO_2 ranges from 50.5 to 62.4 wt%. All samples are potassic. K_2O ranges from ca. 4.5 to 9 wt% and reaches the highest concentrations in samples with intermediate SiO_2 content. K_2O/Na_2O is highest in the most mafic samples ($K_2O/Na_2O > 4$) and decreases with increasing differentiation i.e. decreasing MgO. Fe_{total}, CaO, TiO_2, and P_2O_5 decrease with decreasing MgO whereas Na_2O, Al_2O_3 and SiO_2 increase with decreasing MgO (Fig. 4). The most mafic samples can be considered "ultrapotassic" according to the criteria defined by Foley et al. (1987) with $K_2O/Na_2O > 2$, $K_2O > 3$ wt% and MgO > 3 wt%. All samples are characterized by high concentrations of LILE, Th, U, LREE and HFSE but there are notable differ-

Table 3 Major (in wt %) and trace element (in ppm) composition of syenites (Damara orogen, Namibia)

Sample	M45	M50	M49	M46	M43	M44	M47	M53	M51	M54	M52	98.1.16	98.1.15	98.1.19	98.1.18	98.1.17
SiO_2	50.50	53.10	53.83	53.91	54.95	55.03	55.45	57.71	56.59	58.02	60.98	55.27	59.82	60.24	61.06	62.41
TiO_2	1.40	1.31	0.98	0.90	0.86	1.05	1.02	0.88	0.88	0.83	0.78	0.78	0.65	0.77	0.64	0.76
Al_2O_3	13.45	14.17	13.35	13.47	14.23	14.53	14.38	14.85	14.72	14.42	13.32	14.32	16.25	16.59	15.33	15.69
Fe_2O_3	2.77	2.99	3.03	2.27	1.76	1.73	3.50	3.17	2.64	2.33	2.02	3.17	1.18	2.80	1.43	1.66
FeO	6.95	5.09	4.37	4.72	4.72	4.57	3.45	3.04	3.29	3.68	3.37	3.42	2.82	2.94	3.81	2.71
MnO	0.11	0.15	0.14	0.11	0.09	0.13	0.09	0.09	0.09	0.13	0.08	0.11	0.08	0.09	0.10	0.08
MgO	5.39	4.66	5.24	5.16	4.96	3.92	4.01	3.95	3.33	4.27	3.46	4.86	2.87	1.70	3.32	1.77
CaO	5.71	5.10	6.39	6.59	5.31	5.08	4.81	3.73	3.96	4.94	3.85	5.65	3.78	4.48	5.16	4.55
Na_2O	1.87	2.76	2.64	2.08	2.42	2.25	2.39	2.96	2.37	2.63	3.14	2.16	3.86	3.80	2.70	3.35
K_2O	7.87	7.69	7.16	7.71	7.94	8.35	8.52	8.02	9.08	7.54	6.91	7.29	6.46	5.78	5.11	5.16
P_2O_5	1.12	0.83	0.82	0.80	0.62	0.66	0.65	0.53	0.56	0.55	0.50	0.62	0.47	0.45	0.45	0.36
LOI	0.85	0.72	0.49	1.16	0.69	0.58	0.45	0.95	0.84	0.43	0.46	1.05	0.94	0.93	0.67	0.46
Total	97.99	98.57	98.44	98.88	98.55	97.88	98.72	99.88	98.35	99.77	98.87	98.70	99.18	100.57	99.78	98.96
Sc	24	23	25	21	23	18	16	13	15	14	18	16	17	14	11	14
V	190	185	180	174	164	167	172	127	152	129	150	144	83	136	104	105
Cr	158	119	156	150	86	106	117	94	100	140	119	167	65	16	106	34
Co	27	30	30	34	36	19	21	8	21	15	23	28	16	13	23	15
Ni	79	59	66	70	38	50	60	37	45	67	59	67	28	13	43	15
Zn	66	128	101	52	117	99	66	65	51	73	48	76	53	67	74	47
Ga	22	22	18	16	21	18	20	20	17	17	18	23	15	19	19	21
Rb	538	450	338	361	374	403	383	352	336	228	221	240	249	146	150	150
Sr	830	934	1,043	1,007	1,172	1,094	1,141	739	1,227	920	651	1,072	871	1,498	1,044	1,460
Y	69	55	48	46	42	45	40	45	28	43	34	37	35	43	29	46
Zr	513	568	469	393	267	327	307	386	192	265	270	340	335	402	325	411
Nb	75	71	53	43	29	38	35	40	26	27	25	21	33	44	31	48
Ba	1,570	1,856	2,043	2,097	2,371	2,234	2,732	1,520	2,651	2,021	1,167	2,676	1,708	2,065	1,608	1,400
Pb	60	46	38	54	18	42	45	35	29	28	23	22	30	44	29	35
Th	61	55	38	31	15	55	29	26	20	17	18	10	34	25	18	20
U	13	14	9	8	4	11	7	5	5	4	3	2	6	6	4	5
La	159.20	118.60	216.00	270.00	87.90	205.20	316.40	187.80	360.50	257.40	292.50	89.65	107.99	155.70	104.77	148.70
Ce	330.80	247.60	452.00	500.00	189.40	413.20	662.00	387.20	652.50	538.20	629.00	180.06	207.15	281.26	194.64	273.45
Nd	139.60	99.80	185.00	184.80	84.40	179.60	271.60	145.80	272.50	231.30	246.00	73.34	80.44	103.60	65.57	113.25
Sm	26.25	17.32	32.82	34.48	18.02	33.58	51.60	29.36	51.90	45.33	48.55	14.53	16.04	18.10	12.85	19.40
Eu	5.66	4.33	8.08	7.40	4.11	7.84	11.72	6.14	13.00	10.38	9.70	2.85	3.35	3.70	2.53	3.95
Gd	17.31	12.99	24.86	24.56	11.82	25.32	41.72	20.38	37.65	34.35	38.85	9.70	10.59	12.20	8.08	12.50
Dy	12.58	9.16	18.32	16.86	7.75	17.60	26.08	12.88	24.55	25.41	25.45	6.25	6.66	8.10	5.37	8.25
Er	4.60	3.90	6.40	5.80	3.20	8.20	10.40	6.40	11.50	8.70	9.00	2.40	2.28	2.90	2.50	2.85
Yb	3.30	2.80	4.20	4.80	2.00	5.60	6.80	4.60	9.50	7.20	6.50	1.91	2.16	1.75	2.19	2.15
Lu	0.39	0.37	0.66	0.70	0.27	0.70	1.00	0.64	1.25	1.11	0.85	0.29	0.31	0.25	0.29	0.35
Q	0.00	0.00	0.00	0.00	0.00	0.00	0.00	1.38	0.00	4.35	7.29	0.00	1.77	6.00	11.13	12.32
Or	46.51	45.45	42.31	45.51	46.92	49.35	50.35	47.40	53.66	41.01	40.84	43.09	38.18	34.16	30.20	30.50
Ab	14.89	20.30	20.57	17.45	17.91	19.04	20.22	20.05	20.05	22.25	26.57	18.28	32.66	32.15	22.84	28.34
An	5.06	3.56	3.43	4.65	4.52	4.89	3.35	3.55	2.71	4.32	1.84	7.85	7.94	11.14	11.89	12.54
Ne	0.51	1.65	0.96	0.08	1.39	0.00	0.00	0.00	0.00	0.00	0.00	0.00	0.00	0.00	0.00	0.00
Di	8.96	9.61	15.61	15.66	13.84	10.10	10.17	6.84	8.22	11.07	9.07	12.81	6.26	6.58	8.76	6.24
Hy	0.00	0.00	0.00	0.00	0.00	0.36	0.00	4.18	1.31	5.50	4.43	6.89	7.40	3.03	8.94	3.87
Ol	6.50	5.01	4.07	3.92	2.41	3.34	3.69	0.00	2.22	0.00	0.00	1.22	0.00	0.00	0.00	0.00
Il	0.24	0.32	0.30	0.24	1.63	0.28	0.19	0.19	0.19	0.28	0.17	1.48	1.23	1.46	1.22	1.44
Hem	10.50	8.56	7.89	7.52	2.32	6.81	7.32	6.55	6.31	6.43	5.77	0.00	0.00	4.06	2.07	2.41
Ti	0.00	0.00	0.00	0.00	0.00	2.22	0.88	1.91	1.91	1.68	1.69	0.00	0.00	0.00	0.00	0.00
Ap	2.59	1.92	1.90	1.85	0.00	0.00	1.51	1.23	1.30	1.27	1.16	1.47	1.11	1.07	1.07	0.85
Per	2.17	1.94	1.40	1.32	0.00	0.00	0.95	0.00	0.00	0.00	0.00	0.00	0.00	0.00	0.00	0.00

LOI Loss on ignition

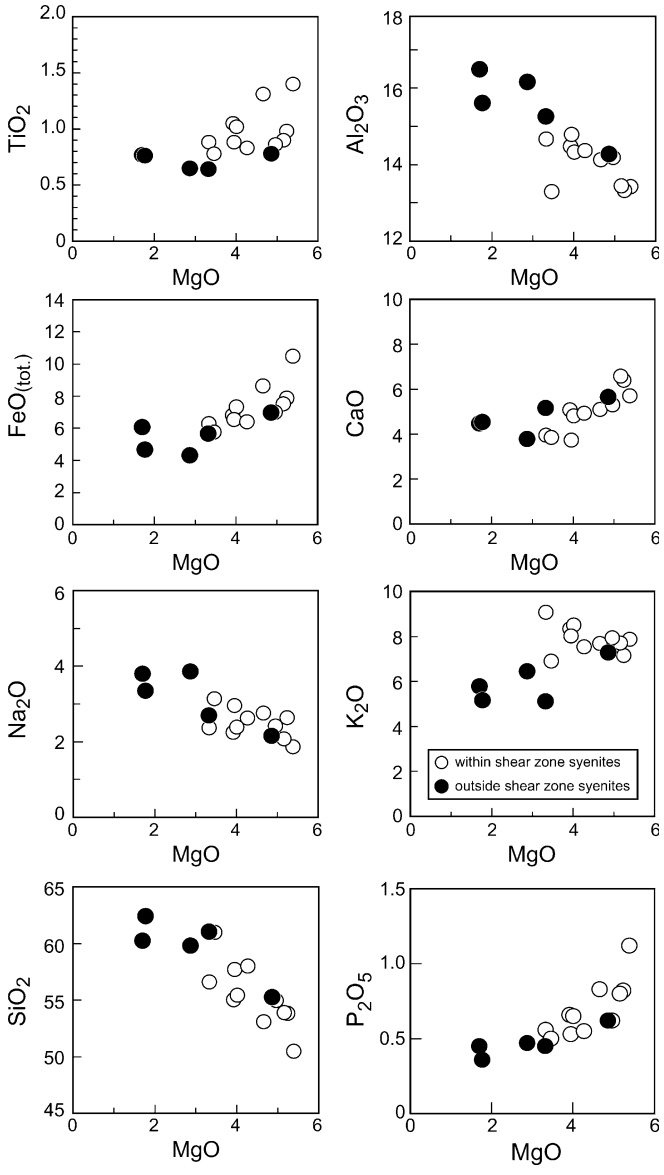

Fig. 4 Major element plots for both types of syenite (Otjimbingwe, Damara orogen, Namibia)

ences between samples from within and outside the shear zone. In samples from within the shear zone Th, U, Y, Zr, Nb and Pb are high and decrease with decreasing MgO, whereas the concentration of these elements in samples from outside the shear zone increases with decreasing MgO. Rubidium is high and decreases with decreasing MgO in both suites. Trace transition metals (Ni, Cr) decrease with increasing SiO_2 (Fig. 5). Primitive mantle-normalized trace element patterns are similar to those of other trace element enriched ultrapotassic to potassic rocks (Foley et al. 1987; Gleason et al. 1994; Miller et al. 1999) with moderate depletions in Th and U (relative to Ba) for syenites from outside the shear zone and strong depletion of Nb, Sr, P and Ti (Fig. 6).

Rare earth element (REE) systematics are also different for the samples from within and outside the shear zone. Generally, REE concentrations are high and increase with decreasing MgO. However, total REE abundances for samples from within the shear zone are distinctly higher with La 500–1,000 and Yb 15–30 times chondrite whereas samples from outside the shear zone have La 300–500 and Yb 9–10 times chondrite (Fig. 7). Consequently, chondrite-normalized La/Yb ratios are different with a rather constant value of about 30 for samples from within the shear zone and 31–46 for samples from outside the shear zone. The most primitive samples from both settings have negligible Eu anomalies (Eu/Eu*: 1.0–0.8).

Strontium, Nd, Pb and O isotopes

The results of the Sr, Nd, Pb and O isotope analyses are reported in Table 4. Samples from within the shear zone and from outside the shear zone have unradiogenic Nd isotope composition (initial ϵ Nd: -5.5 to -3.8 for samples from within and -7.9 to -4.7 for samples from outside the shear zone). Initial $^{87}Sr/^{86}Sr$ ratios range from 0.70665 to 0.70767 for samples from within the shear zone and from 0.70778 to 0.70955 for samples from outside it (Fig. 8). For samples from within the shear zone, initial ϵ Nd values become less radiogenic and Sr isotope compositions become more radiogenic with decreasing MgO. For samples from outside the shear zone, the opposite is the case (Fig. 9). Generally, all syenite samples show rather high $\delta^{18}O$ values whereby the variation of $\delta^{18}O$ for samples from within the shear zone is between 8.6 and 9.3‰ and between 8.8 and 9.7‰ for samples from outside the shear zone. Oxygen isotope values increase with decreasing MgO (Fig. 9). These values are similar to those reported for other Damaran mafic rocks (7.8–9.9‰; Haack et al. 1982; Jung et al. 2002) and approach values reported from unfractionated basement-derived granodiorites from the Damara belt (Jung et al. 2003). Despite the highly alkaline and potassic nature of the syenites, the values of the most mafic samples are more typical of mafic crustal rocks than for mafic rocks that contain a mantle component. However, all of them are lower than values reported from most Damaran granites and upper crustal metasedimentary rocks, which can have very high values up to15 ‰ (Haack et al. 1982; Jung et al. 2001, 2003).

Like the Nd and Sr isotope composition, $^{206}Pb/^{204}Pb$, $^{207}Pb/^{204}Pb$ and $^{208}Pb/^{204}Pb$ ratios show some variation with major element composition. The Pb isotope values increase with decreasing MgO for samples from outside the shear zone but the opposite is true for samples from within the shear zone. For both suites, $^{207}Pb/^{204}Pb$ ratios decrease with decreasing ϵ Nd values and increasing initial $^{87}Sr/^{86}Sr$ values. The $^{206}Pb/^{204}Pb$, $^{207}Pb/^{204}Pb$ and $^{208}Pb/^{204}Pb$ ratios obtained on acid-leached K-feldspar separates for both suites are slightly more radiogenic than average upper crust with $\mu = 9.74$ and $\kappa = 4.0$ (Fig. 10; Stacey and Kramers 1975).

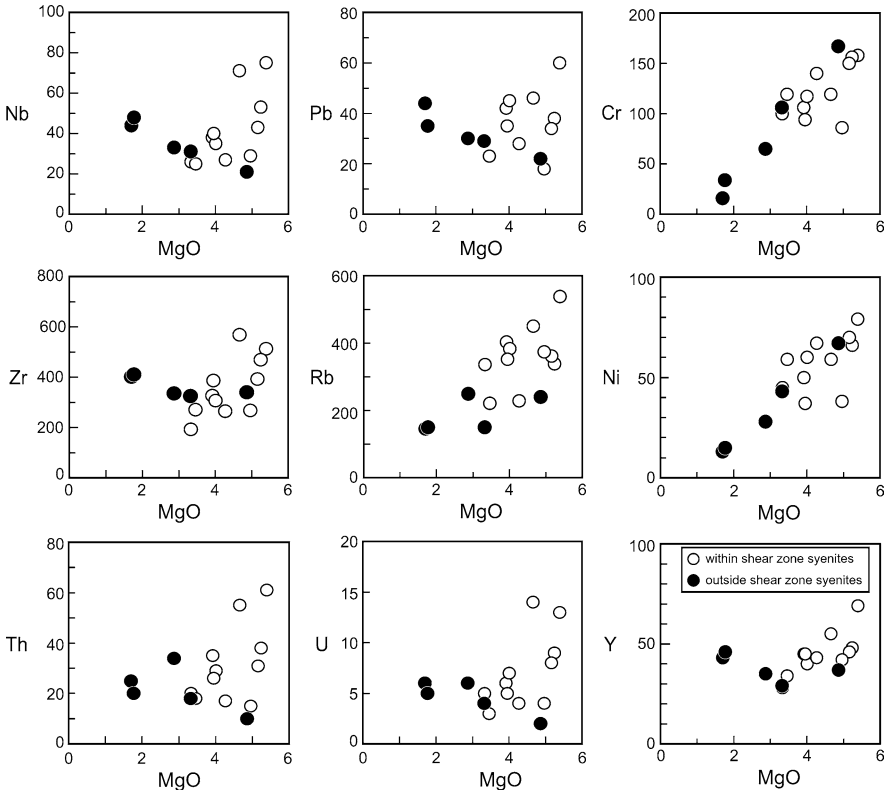

Fig. 5 Selected trace element plots for both types of syenite (Otjimbingwe, Damara orogen, Namibia)

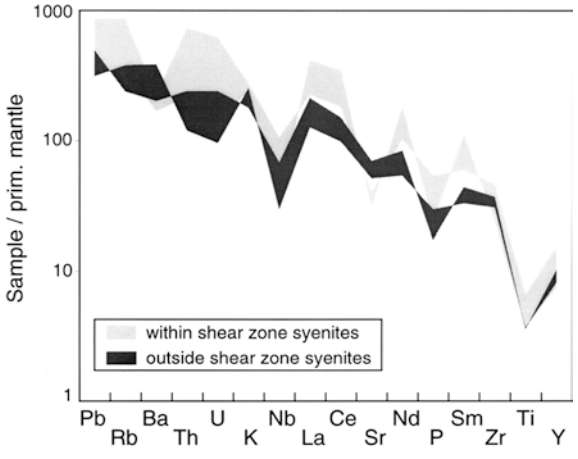

Fig. 6 Primitive-mantle normalized trace element diagram for both suites of syenites (Otjimbingwe, Damara orogen, Namibia)

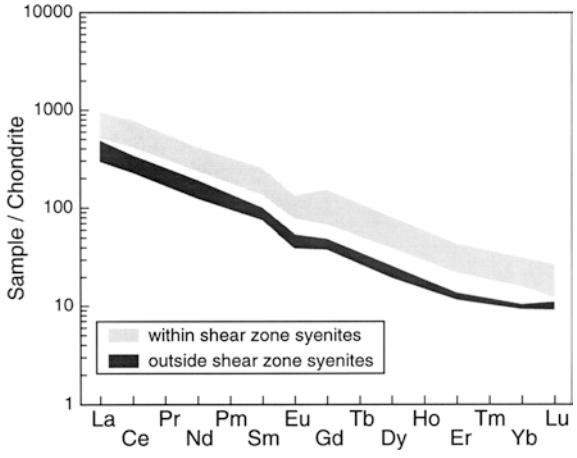

Fig. 7 Chondrite-normalized rare earth element plots for both types of syenite. Normalization factors according to Boynton (1984)

Discussion

Simple models for the evolution of strongly potassic rocks that erupt through, or intrude into, the continental crust do not exist. The generation and evolution of these rocks is controlled by the source mineralogy, the degree of melting, the fractional crystallization history and the likely crustal contamination. The isotope composition of many syenites is heterogeneous and this can be related to source heterogeneity or crustal contamination or both. In order to place constraints on the composition of the mantle source and the melting conditions it is also necessary to evaluate the effects of crystal fractionation, with and without assimilation, on the initial magma composition.

Fractional crystallization processes

Both suites of syenites are distinct, but for all samples a general fractional crystallization trend is suggested by decreasing FeO_{total}, CaO, P_2O_5, Cr, Ni, Zr, and Rb

Table 4 Rb–Sr, Sm–Nd, Pb and O isotope data from Otjimbingwe syenites (Damara orogen, Namibia)

	$^{87}Sr/^{86}Sr$ (m)	$^{87}Sr/^{86}Sr$ (i)	$^{87}Rb/^{86}Sr$	Rb (ppm)	Sr (ppm)	$^{206}Pb/^{204}Pb$	$^{207}Pb/^{204}Pb$	$^{208}Pb/^{204}Pb$
M45	0.720383(18)	0.706648	1.8532	542.9	848.6	18.054	15.669	38.326
M50	0.717004(15)	0.706821	1.3740	439.4	925.9	18.033	15.634	38.233
M49	0.713995(11)	0.706971	0.9477	335.0	1023	18.084	15.645	38.252
M46	0.714553(14)	0.707059	1.0112	350.6	1004	18.316	15.691	38.420
M43	0.713877(10)	0.706999	0.9280	372.6	1163	18.089	15.641	38.246
M44	0.714904(11)	0.707137	1.0480	400.2	1105	18.073	15.649	38.271
M47	0.714079(11)	0.707120	0.9390	366.4	1129	18.107	15.659	38.285
M53	0.717247(14)	0.707353	1.3350	342.5	743.1	17.907	15.628	38.198
M51	0.712816(09)	0.707057	0.7770	331.1	1234	17.775	15.609	38.101
M54	0.713323(11)	0.707672	0.7625	225.3	855.2	17.848	15.617	38.154
M52	0.714007(10)	0.706981	0.9480	198.1	604.8	17.919	15.621	38.328
98.1.16	0.714258(13)	0.709553	0.6348	237.9	1085	17.762	15.614	38.209
98.1.15	0.714256(19)	0.708364	0.7950	239.2	870.9	17.804	15.639	38.462
98.1.19	0.709868(10)	0.707782	0.2814	151.8	1561	17.905	15.736	38.686
98.1.18	0.711551(13)	0.708586	0.4000	142.9	1034	17.820	15.649	38.503
98.1.17	0.710289(13)	0.708125	0.2920	159.0	1576	17.819	15.680	38.436

	$^{143}Nd/^{144}Nd$(m)	$^{143}Nd/^{144}Nd$(i)	$^{147}Sm/^{144}Nd$	Sm (ppm)	Nd (ppm)	ϵ Nd (520 Ma)	T_{DM}	$\delta^{18}O$
M45	0.512143(12)	0.511751	0.1152	27.41	143.8	−4.2	1.4	8.90
M50	0.512151(11)	0.511761	0.1146	20.90	110.3	−4.0	1.4	8.60
M49	0.512149(10)	0.511766	0.1124	33.87	181.7	−3.9	1.3	8.40
M46	0.512175(14)	0.511772	0.1182	32.58	166.6	−3.8	1.4	8.60
M43	0.512143(12)	0.511742	0.1178	14.89	76.39	−4.4	1.4	8.60
M44	0.512106(09)	0.511704	0.1179	32.52	166.7	−5.1	1.5	8.80
M47	0.512126(11)	0.511739	0.1135	44.61	237.6	−4.5	1.4	9.00
M53	0.512114(10)	0.511735	0.1112	27.90	151.9	−4.5	1.4	8.90
M51	0.512102(12)	0.511713	0.1143	50.90	269.2	−5.0	1.4	9.10
M54	0.512112(13)	0.511715	0.1165	42.29	219.4	−4.9	1.4	8.60
M52	0.512116(15)	0.511730	0.1134	47.72	254.5	−4.7	1.4	9.30
98.1.16	0.511937(11)	0.511563	0.1098	13.60	74.85	−7.9	1.6	8.75
98.1.15	0.512032(11)	0.511665	0.1078	15.65	87.76	−5.9	1.4	9.60
98.1.19	0.512074(10)	0.511728	0.1017	18.20	108.2	−4.7	1.3	9.45
98.1.18	0.511946(12)	0.511591	0.1043	13.31	77.11	−7.4	1.5	9.45
98.1.17	0.512044(11)	0.511698	0.1016	20.24	120.5	−5.3	1.4	9.65

Uncertainties for the $^{87}Sr/^{86}Sr$ and $^{143}Nd/^{144}Nd$ are two σ (mean) in the last two digits. ϵ Nd values at the time of intrusion are calculated relative to CHUR with present-day values of $^{143}Nd/^{144}Nd = 0.512638$ and $^{147}Sm/^{144}Nd = 0.1966$ (Jacobson and Wasserburg 1980). Nd model ages (T_{DM}) calculated with a depleted mantle reservoir and present-day values of $^{143}Nd/^{144}Nd = 0.513144$ and $^{147}Sm/^{144}Nd = 0.222$ (Michard et al. 1985)
m measured, *I* initial

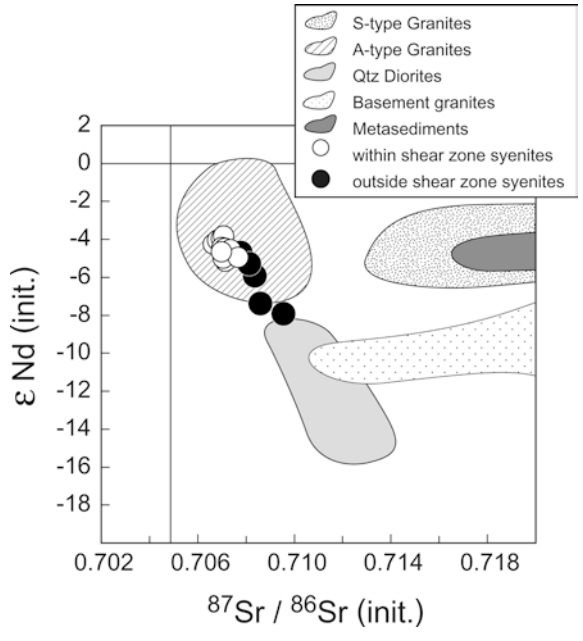

concentrations and increasing Na_2O and Al_2O_3 concentrations with decreasing MgO (Figs. 4 and 5). For samples from within the shear zone, the concentration of K_2O generally decreases with decreasing MgO although some fractionated samples show higher K_2O concentrations at comparatively low MgO concentrations. For samples from outside the shear zone, K_2O generally decreases with decreasing MgO. Barium and Sr show some scatter, although samples with high K_2O also have high Ba, but generally low Sr concentrations (Table 3). Concentrations of Nb display two trends (Fig. 5). For samples from within the shear zone, Nb decreases with decreasing MgO, whereas for the samples from outside the shear zone concentration of Nb increase with increasing differentiation. These variations in Nb concentrations may indicate a dominant

◀

Fig. 8 Initial ϵ Nd vs. initial $^{87}Sr/^{86}Sr$ diagram for both types of syenite. Fields for other crustal rocks from the Damara orogen are from Jung et al. (1998b, 2001, 2002, 2003, unpublished data)

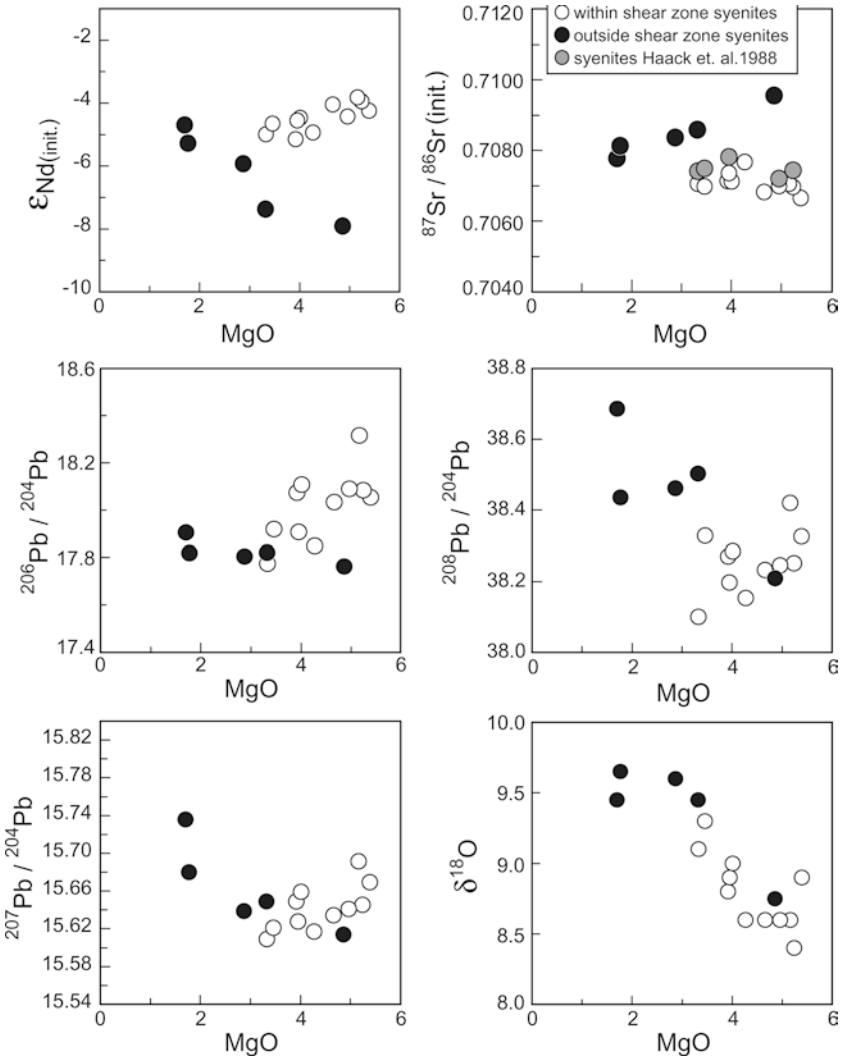

Fig. 9 Initial ϵ Nd, $^{87}Sr/^{86}Sr$, $^{206}Pb/^{204}Pb$, $^{207}Pb/^{204}Pb$, $^{208}Pb/^{204}Pb$ and $\delta^{18}O$ vs. MgO for both types of syenite. The trends are best explained by assimilation of felsic rocks during fractional crystallization. Note that in the case of the syenites from within the shear zone the contaminant must be more radiogenic in Sr and less radiogenic in Nd isotope composition whereas for the syenites from outside the shear zone the opposite is true

role for titanite during the early stages of differentiation in the case of the syenites from within the shear zone. Concentrations of REE increase with decreasing MgO for the samples from within the shear zone (Table 3), although there is some variation in the fractionation of LREE to HREE. With increasing differentiation, the Eu concentration increases although a weak negative Eu is developed. The most differentiated sample has a slightly positive Eu anomaly suggesting plagioclase accumulation. Increasing concentrations of REE during differentiation support the dominance of clinopyroxene and amphibole fractionation. The scatter of Ba and Sr, at least in the samples from outside the shear zone, the constant concentration of Ga and the only weakly developed negative Eu anomaly indicate that fractionation of plagioclase was of minor importance.

In conclusion, the relatively large range in SiO_2 and MgO combined with distinct geochemical variations suggests that crystal–liquid fractionation played an important role in the petrogenesis of the syenites. However, the ubiquitous presence of large K-feldspar phenocrysts in most samples suggests that separation of these early crystallized crystals was incomplete. In this case, the variations of TiO_2, Ni, Cr etc. with MgO are due to fractionation of early crystallized mafic minerals (clinopyroxene, amphibole, sphene, titanomagnetite), whereas the high concentrations of Ba and K_2O in samples with intermediate SiO_2 contents may point to K-feldspar accumulation in the crystallization history.

Sources of the syenites

Despite the apparent crustal contamination, the geochemical composition of the syenites studied here indicate that they were derived from a source enriched in Rb and LREE relative to Bulk Earth. The radiogenic isotope data do not clearly distinguish between a pure mantle or crustal source for the Otjimbingwe syenites. Initial $^{87}Sr/^{86}Sr$ ratios are slightly elevated relative to Bulk Earth, but do not approach the highly radiogenic values from Damaran crustal rocks. Initial ϵ Nd values are moderately negative and similar to most synorogenic upper crustal granites from the Central Damara orogen (McDermott et al. 1996; Jung et al.

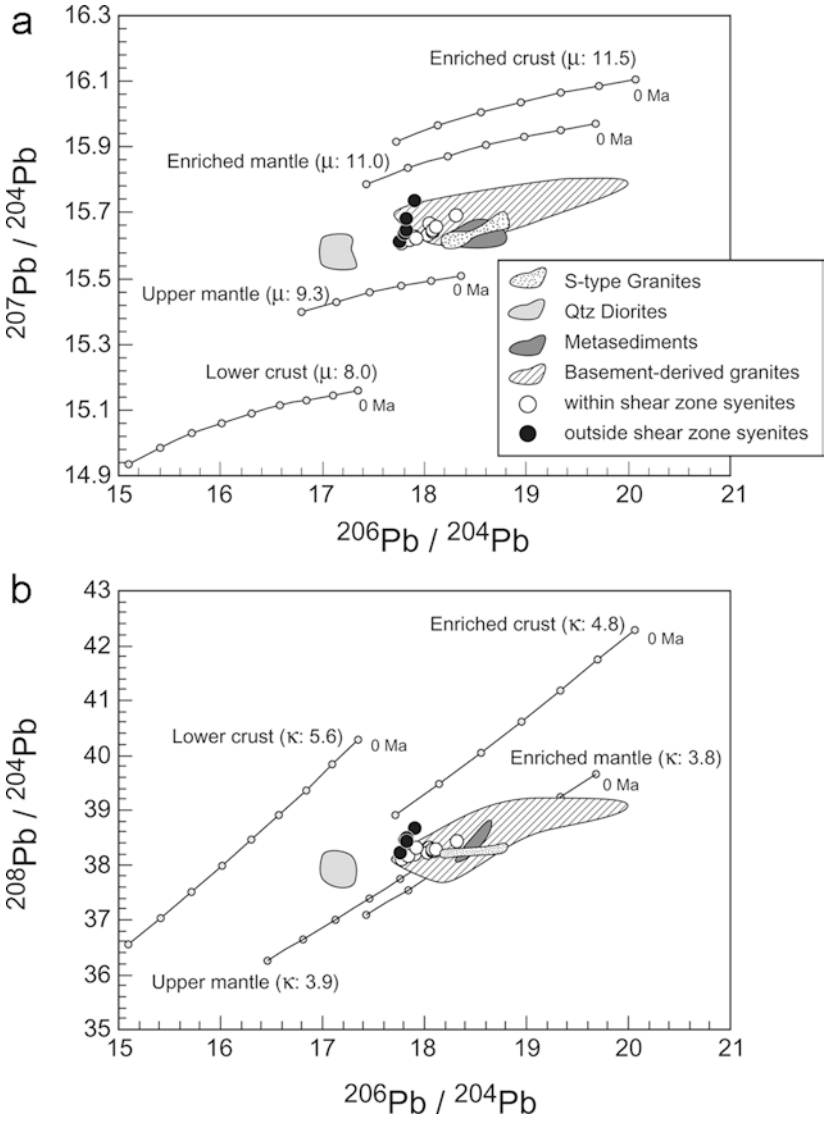

Fig. 10a, b Plot of **a** $^{207}Pb/^{204}Pb$ and **b** $^{208}Pb/^{204}Pb$ vs. $^{206}Pb/^{204}Pb$ isotope ratios of leached K-feldspar from both types of syenite. The *different curves* represent hypothetical Pb growth curves with different μvalues. *Tick marks* represent 200 Ma intervals. Fields for other crustal rocks from the Damara orogen are taken from Jung et al. (1998b, 2001, 2002, 2003, unpublished data)

2001). Depleted mantle model ages are also similar (1.3–1.6 Ga) for these rock types and the Otjimbingwe syenites, but are not characteristic for average Damaran felsic lower crust with Nd model ages up to 2.5 Ga (McDermott et al. 1996; Jung et al. 2003). A derivation from Damaran depleted mafic lower crust is unlikely because this crust also has significantly older Nd model ages up to 2.2 Ga and a strongly unradiogenic Pb isotope composition (Jung et al. 2002). The model ages alone do not rule out average Damara crust as a potential source because some fractionation of Sm relative to Nd has been observed elsewhere (e.g., Patchett 1992) and attributed to the presence of minerals with high Sm/Nd ratios (e.g. garnet, amphibole, zircon) in the residue. Such fractionation can lead to erroneously young Nd model ages. However, the apparent lack of fractionation of Sm relative to Nd results in similar $^{147}Sm/^{144}Nd$ ratios for most unfractionated granites from the Damara orogen (0.10–0.14; McDermott et al. 1996; Jung et al. 2001, 2003) and the Otjimbingwe syenites (0.10–0.12), and do not indicate strong involvement of minerals with high Sm/Nd during melting. Overall, the Nd–Sr isotope composition of the syenites requires a source with moderately high time-integrated Rb/Sr, but low Sm/Nd ratios.

Lead isotopes are very sensitive indicators of source characteristics and the involvement of crustal material during magma genesis. The variation in Pb isotopes can be used to constrain the effects of crustal contamination, however, even the values obtained on leached K-feldspar from the least contaminated samples are distinctly higher than likely values for asthenospheric mantle at that time and plot slightly above the $^{207}Pb/^{204}Pb$–$^{206}Pb/^{204}Pb$ and $^{208}Pb/^{204}Pb$–$^{206}Pb/^{204}Pb$ evolution curves with $\mu = 9.3$ and $\kappa = 3.9$. Furthermore, the $^{206}Pb/^{204}Pb$ ratios are slightly lower than those observed in leached K-feldspar from orogenic granites and metasedimentary rocks from the Damara orogen (Fig. 10), excluding average Damaran igneous or metasedimentary crust as a potential source. It is therefore

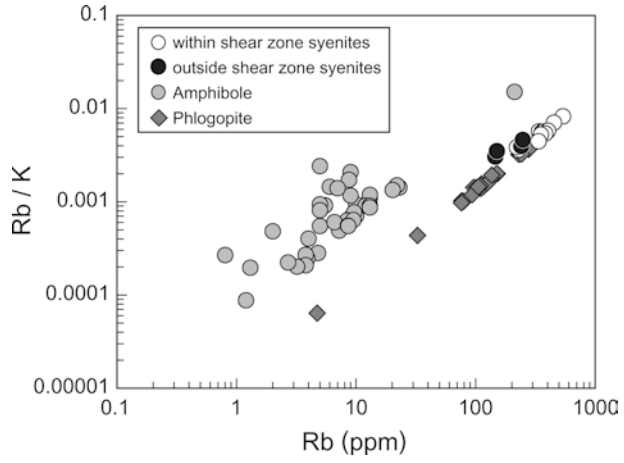

Fig. 11 Rb/K vs. Rb plot for both suites of syenite. Phlogopite and amphibole composition from Irving and Frey (1984), O'Reilly et al. (1991), Adam et al. (1993), Ionov and Hofmann (1995), and T. Green (personal communication)

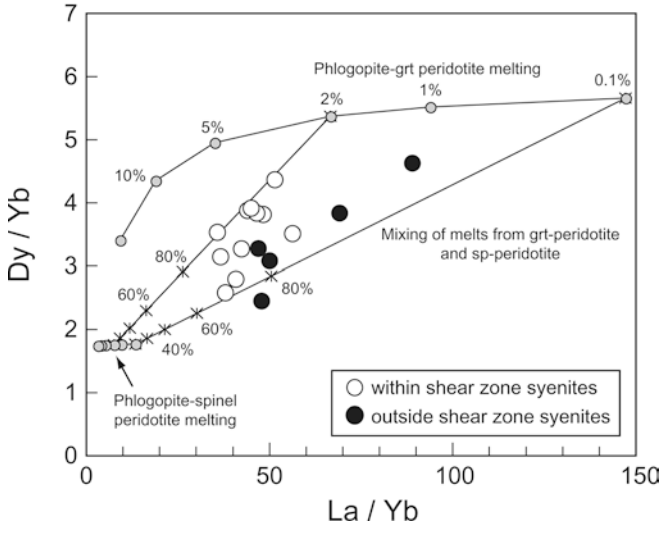

Fig. 12 La/Yb vs. Dy/Yb for the syenites from Otjimbingwe. Non-modal batch melting curves were calculated for phlogopite-grt-bearing harzburgite and phlogopite-spinel-bearing harzburgite. Partition coefficients were taken from McKenzie and O'Nions (1991). Sources were phl-grt harzburgite (cpx10, opx30, ol20, phl20, grt20) which melts in the proportions (cpx10, opx10, ol10, phl30, grt40) and garnet-free phl-harzburgite (cpx20, opx40, ol30, sp3, phl7) which melts in the proportions (cpx30, opx20, ol9, sp1, phl40). Points of the melting curves are 0.1, 1, 2, 5, 10, and 20%. Additionally, *mixing curves* are shown that represent mixing between relatively large melt fractions from the garnet facies with relatively smaller fractions from the spinel facies

concluded that the syenites come from a pre-Pan African source with elevated time-integrated U/Pb and Th/U ratios. One possible model is to ascribe the Pb isotope compositions to a metasomatized lithospheric component that was isolated for a considerable period of time from the convecting upper mantle before the partial melting event. Mixing of different isotopic compositions from a variety of sources including the depleted asthenosphere and enriched lithosphere is then possible (Nelson et al. 1986). High and positively correlated La/Nb and Ba/Nb ratios suggest some affinity to potassic lamproites, whose source probably resides within the subcontinental lithosphere. The samples with the highest MgO content have low Ce/Pb ratios that correlate with high ^{207} Pb/^{204}Pb ratios. These features also indicate that typical asthenospheric sources were not involved, and the source of the syenites is probably in the lithosphere.

One likely source for the incompatible trace element enrichment of the proposed lithospheric mantle could be a subduction-related component. The presence of negative Nb and Ti anomalies in primitive mantle-normalized diagrams (Fig. 6) could indicate the presence of such a component, probably due to the effect of residual titanates (Foley and Wheller 1990). The most mafic syenites have low Ti/Y ratios (122–143), high Rb/Ba (0.24) and high Rb/Sr (0.48–0.65) ratios. They also have low Ce/Pb (ca. 5), low Sr/Nd (6–10), low Nb/La (0.47–0.60) but elevated Sr/Ce (0.27–0.40) ratios and high δ^{18}O values between 8.6 and 8.9‰. Overall, the combination of geochemical features evaluated above is suggestive of continental material subducted back into the mantle.

Constraints on source mineralogy and partial melting processes

Current models for the generation of strongly potassic rocks invoke a veined mantle source (Foley 1992). The vein mineralogy should consist of hydrous (e.g., phlogopite, amphibole, apatite) and anhydrous (e.g., zircon) mineral phases enriched in incompatible trace elements. The primitive mantle, most MORB, OIB and non-orogenic lamproites have low Rb/Sr (< 0.1) and low Rb/Ba (0.03–0.1) ratios indicating that partial melting processes giving rise to these magmas do not fractionate Rb/Ba significantly (Hawkesworth et al. 1985). Otjimbingwe syenites from within the shear zone have higher Rb/Sr (0.25–0.65) and Rb/Ba (0.11–0.34) ratios. Alkaline rocks with high Rb/Sr and Rb/Ba ratios are often characterized by low Ti/K ratios, a feature also shown by the syenites studied here (Ti/K: 0.07–0.13). These geochemical features have been attributed to the presence of phlogopite in the mantle source of alkaline magmas. Relative to other mantle minerals, phlogopite is H_2O-rich and can serve as an agent for hydrous mantle metasomatism (Erlank et al. 1987). Additionally, negatively correlated U/Pb and K/Nb ratios in ultrapotassic rocks have been attributed to the presence of a K-bearing mineral phase that fractionates U/Pb (Hawkesworth et al. 1990). In the Otjimbingwe syenites, high K/Nb (870–2,900) and low U/Pb (0.06–0.30) are associated with high Rb/Sr, suggesting the presence of some residual phlogopite in the source region. Furthermore, in Rb vs. Rb/K space (Fig. 11) the samples display a clear trend towards phlogopite analyses from the literature, and quite different from amphibole.

Additional mineralogical characteristics of the mantle source of the Otjimbingwe syenites can be illustrated using La/Yb and Dy/Yb ratios, which have been used to distinguish between melting in the garnet or spinel stability field (Thirlwall et al. 1994). The La/Yb ratio for the most primitive syenites from both localities is high and rather uniform between 45 and 50 (Fig. 12). Melting in the garnet stability field produces large variation in La/Yb ratios at low degrees of melting whereas melting in the presence of spinel leaves this ratio rather unchanged (Fig. 12). Partial melting curves as well as mixing curves between melts from a garnet-bearing and garnet-free source are shown in Fig. 12. From the data, it is obvious that the variation of La/Yb and Dy/Yb cannot be generated by low-degree melting of a hypothetical LREE-enriched source solely in the garnet or spinel stability field. Instead, the variation in Dy/Yb and La/Yb suggests mixing of melts from different reservoirs. In this scenario the contribution of melts from the garnet stability field during the initial stages of melting is high for the syenites from within the shear zone but low for the syenites from outside the shear zone.

Contamination processes

Based on the variation of major and trace element abundances fractional crystallization, together with limited accumulation of predominantly K-feldspar, is considered as the predominant process for the evolution of the syenites from Otjimbingwe. However, it is likely that the majority of continental syenites were generated by interaction between mantle-derived alkali basaltic melts and pre-existing continental crust. Fitton (1987) and Foland et al. (1993) proposed that assimilation of continental crust is essential for a nepheline-normative magma to evolve across the thermal divide in the quartz–nepheline–kalsilite system in order to produce a qtz-normative syenitic melt. Neodymium, Sr, Pb and O isotope data reveal a noticeable role of crustal contamination in the generation of the more evolved quartz-normative syenite magmas, most probably via a concurrent crustal assimilation and fractional crystallization process (AFC; DePaolo 1981). Calculation of AFC curves are model dependent, because they require assumptions about the fractionating mineral assemblage and mineral-melt distribution coefficients, the concentrations of the respective trace elements in the starting melt and the contaminant as well as the ratio of assimilation to fractional crystallization (*r*-value).

As a first approximation, the Pb isotope composition of the leached feldspar separates can be used to place constraints on the likely contaminants of both syenite suites. In the $^{206}Pb/^{204}Pb$ vs. $^{207}Pb/^{204}Pb$ diagram (Fig. 10) the syenite samples plot between a common upper mantle composition and enriched mantle or crustal sources. This slightly enriched Pb isotope composition, relative to average upper crustal rocks according to Stacey and Kramers (1975), is interpreted to reflect an enriched lithospheric upper mantle source. For the syenites from within the shear zone, extrapolation back to a hypothetical mantle-derived alkaline melt with 10 wt% MgO suggests that this enriched mantle should have ϵ Nd of -2 and $^{87}Sr/^{86}Sr$ close to 0.705 which are reasonable values for an enriched lithospheric upper mantle component. Combined assimilation-fractional crystallization processes led to lower $^{206}Pb/^{204}Pb$ and $^{207}Pb/^{204}Pb$ ratios (see Fig. 9). It is therefore reasonable to infer a lower crustal contaminant with $\mu = 8.0$ (Fig. 10). Combined AFC model calculations using Sr, Nd and Pb isotopes support the model of lower crustal assimilation. The lower crustal end member has ϵ Nd of -30 and $^{87}Sr/^{86}Sr$ of 0.735 similar to the values of the pre-Pan African basement beneath the Damara-Kaoko belt (Seth et al. 2002). Bulk Kd for Sr and Nd were assumed to be 1.5 and 0.8 because the concentrations of these elements decrease and increase, respectively, during differentiation (Table 3). In order to model the elemental concentration of Nd and Sr in the most differentiated melt, the rate of assimilation to fractional crystallization was set to 0.7, in agreement with recent estimates (Reiners et al. 1995). The resulting amount of assimilation is close to 10% (Fig. 13). In terms of $^{206}Pb/^{204}Pb$ vs. ϵ Nd, assimilation can be modeled using a Pb isotope composition for the upper mantle source of $^{206}Pb/^{204}Pb = 18.6$ and for the lower crustal component of $^{206}Pb/^{204}Pb = 15.8$ (Fig. 12). Bulk Kd for Pb was fixed at 1.5 and the amount of assimilation is again close to 10%. Similarly, increasing $\delta^{18}O$ values with decreasing MgO support the model of crustal assimilation.

The syenite samples from outside the shear zone can be adequately described as a mixture of a moderately enriched upper mantle source ($\mu = 9.3$) with an enriched crustal source ($\mu = 11.5$; Fig. 10), because during AFC processes $^{207}Pb/^{20}Pb$ ratios increase with increasing differentiation (Fig. 9). For these samples AFC model calculations give distinct results. During assimilation, Pb isotope ratios increase while ϵ Nd values become more radiogenic and $^{87}Sr/^{86}Sr$ ratios become less radiogenic, which is not compatible with a highly enriched crustal source with inferred low Sm/Nd and high Rb/Sr ratios (Fig. 9). The mafic lower crust as a potential candidate may have high Sm/Nd and low Rb/Sr but it rarely has high U/Pb at the same time (e.g., Thirlwall and Burnard 1990). Therefore, mafic lower crust seems not to be a viable candidate. Bulk Kd values for Sr were set at 0.9 and for Nd at 0.7, because concentrations of these elements increase during differentiation indicating that they behave as moderately incompatible elements. In order to model the elemental concentration of Nd and Sr in the most differentiated melt, the rate of assimilation to fractional crystallization was again fixed at 0.7. Model calculations suggest that contamination of the parental syenite from outside the shear zone with an E-MORB-like contaminant with ϵ Nd $= +9$ and $^{87}Sr/^{86}Sr = 0.706$ may produce the observed isotope pattern (Fig. 13). Additionally, in ϵ Nd vs. $^{206}Pb/^{204}Pb$ space (Fig. 13) the

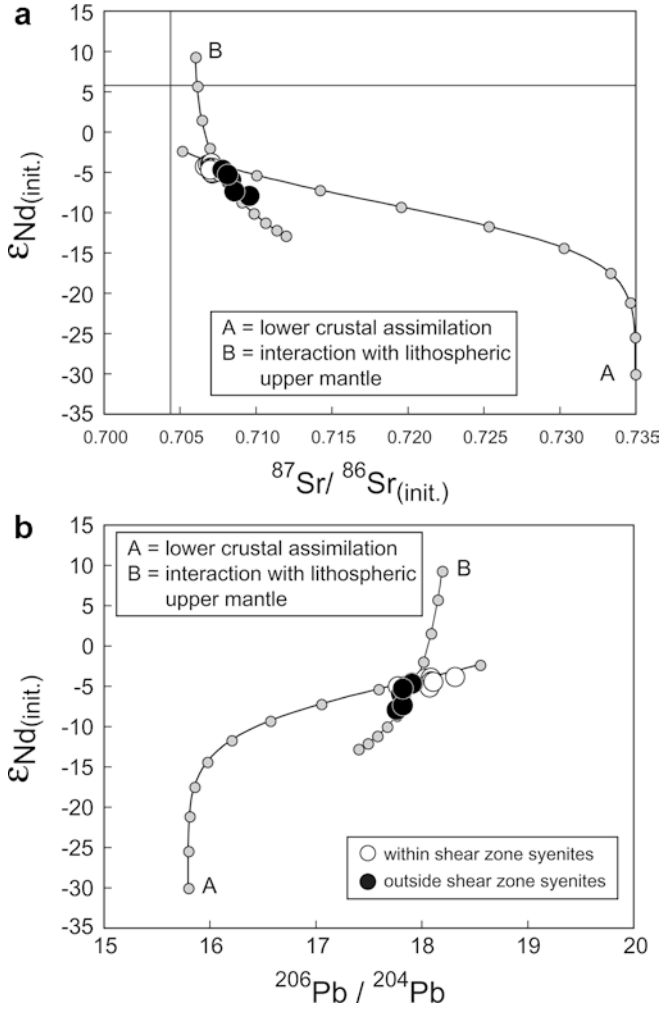

Fig. 13a, b AFC calculations using initial ϵ Nd vs. **a** $^{87}Sr/^{86}Sr$ and **b** $^{206}Pb/^{204}Pb$ isotope composition for both syenite suites. In the case of the syenites from within the shear zone (case A) assimilation is best modeled with a parental melt (i.e. the most primitive sample M45) with 140 ppm Nd ($^{143}Nd/^{144}$ Nd: 0.511750, ϵ $Nd_{(520Ma)}$:−4), 830 ppm Sr ($^{87}Sr/^{86}Sr_{(520Ma)}$: 0.706) and 60 ppm Pb ($^{206}Pb/^{204}Pb$: 18.20). The hypothetical contaminant has 30 ppm Nd ($^{143}Nd/^{144}Nd$: 0.510400, ϵ $Nd_{(520Ma)}$: −30, 200 ppm Sr ($^{87}Sr/^{86}Sr_{(520Ma)}$: 0.735, 40 ppm Pb, $^{206}Pb/^{204}Pb$: 15.80). For the samples from outside the shear zone (case B), the parental melt (i.e. sample 98.1.16) has 70 ppm Nd ($^{143}Nd/^{144}Nd$: 0.511500, $\epsilon Nd_{(520Ma)}$:−8), 1,070 ppm Sr ($^{87}Sr/^{86}Sr_{(520Ma)}$: 0.710) and 20 ppm Pb ($^{206}Pb/^{204}Pb$: 17.76). The hypothetical contaminant has 10 ppm Nd ($^{143}Nd/^{144}Nd$: 0.512450, ϵ $Nd_{(520Ma)}$: + 9, 500 ppm Sr ($^{87}Sr/^{86}Sr_{(520Ma)}$: 0.706, 5 ppm Pb, $^{206}Pb/^{204}Pb$: 18.2). The *r*-value (ratio of assimilation to fractional crystallization) was 0.7 in both cases. Kds for Sr, Nd and Pb were 0.8, 1.5 and 1.5 for samples from within the shear zone and 0.7, 0.9 and 0.8 for samples from outside the shear zone. *Tick marks* represent 10% intervals

contaminant must have a $^{206}Pb/^{204}Pb$ isotope composition of ca. 18.2, which is not unusual for an inferred E-MORB-like composition at 500 Ma. In this case the bulk Kd for Pb was chosen to be 0.8. The unusual isotope evolution towards more radiogenic ϵ Nd values, less radiogenic $^{87}Sr/^{86}Sr$ ratios and more radiogenic $^{206}Pb/^{204}Pb$ ratios for the syenites from outside the shear zone can be explained by interaction of the parental syenite magma with a lithospheric mantle component of E-MORB composition (or a partial melt thereof). Since the lithosphere is thought to be generally depleted, it must have undergone secondary enrichment by the emplacement of enriched fluids. Such a process would lead to enrichment of U which, over time would cause high Pb isotope ratios. Secondary enrichment of Rb was apparently minor because the Sr isotope composition of the contaminated samples is less radiogenic than those in the inferred less contaminated samples. Increasing oxygen isotope values with decreasing MgO indicates that the contaminant has high $\delta^{18}O$ values probably due to secondary enrichment processes.

In conclusion, the syenites from within the shear zone originated by partial melting from a moderately enriched lithospheric source and were subsequently modified by contamination with a felsic lower crustal component. In contrast, the isotope evolution of the samples from outside the shear zone is the result of interaction of two different lithospheric upper mantle domains with different Rb/Sr, Sm/Nd and U/Pb ratios.

Tectonic significance

One of the most important factors in the evolution of the Otjimbingwe syenites is the intimate association of the syenites with a prominent, large-scale shear zone which may have promoted fast ascent and intrusion of the melts. In a plate-tectonic context, a correlation between alkaline magmatism and changes in the direction of micro-plate movements between the southern and the central part of the Damara orogen can be suggested, provoking reactivation of lithospheric shear zones and rifting within these micro plates. If such reactivation caused a reversal in the sense of movement, the associated faults opened and propagated as tensional faults. This would have allowed fracturing through the continental crust causing pressure release, channeling of volatiles, partial melting and generation of magmas from the subcontinental lithospheric mantle. The Damaran syenites display all features of anorogenic within-plate magmatism, despite their appearance close to the peak of the Damaran high-grade metamorphism and their location along a major suture zone. Tectonically, the syenites intruded along the Okahandja shear zone which is probably one of the oldest shear zones in the Damara belt. The intrusion of the syenites was probably accompanied by a change in the stress field which renewed transcurrent movements along lithospheric mega-shear zones. In this model, access to new mantle sources is due to the rise of mantle material to shallow depths beneath continental lithosphere after rupture of the cold lithospheric plate. While the source of the alkaline rocks is in the lithospheric mantle, their location is controlled by the structure, composition and dynamics of the overlying continental crust.

Summary and conclusion

Alkaline igneous rocks can be generated in almost all tectonic settings except mid-ocean ridges. Alkaline igneous rocks formed in subduction-related regimes (or those derived from sources previously modified by a subduction zone component) usually show distinctive depletion of HFSE and evolved isotopic compositions with high initial $^{87}Sr/^{86}Sr$ and low ϵ Nd (Nelson and McCulloch 1989; Rogers et al. 1985). In contrast, alkaline rocks generated in rift-related environments do not show depletion of HFSE and have essentially primitive isotopic signatures (Menzies 1987; McDonough et al. 1985). These geochemical and isotopic differences must be attributed to different mantle sources. The subduction zone-related magmas can be derived from metasomatized mantle wedges above the deepest part of the subduction zone whereas the rift-related magmas are interpreted as being related to garnet-present low-degree partial melting of upwelling asthenosphere. In this case, upwelling asthenospheric material can also causes heat transfer into the veined lithosphere which may result in melting of material with a lower melting temperature than common upper mantle lherzolite. For the Otjimbingwe syenites, there is good evidence for the involvement of a subduction zone component (enriched isotopic compositions, high La/Nb, Ba/Nb, Rb/Ba, Rb/Sr, Sr/Ce and low Ce/Pb, Sr/Nd, Ti/Y). However, due to the absence of an active Pan-African subduction zone in this part of the orogen, the apparent subduction zone component is likely an ancient feature of the subcontinental upper mantle which is also supported by the Nd model ages between 1.3 and 1.5 Ga. Such an upper mantle can be produced via metasomatism of the depleted mantle by slab-derived components during previous episodes of major continental formation. For the syenites from within the shear zone initial ϵ Nd values are moderately unradiogenic (ϵ Nd: -4) and if contamination with an ancient crustal component is responsible for this isotopic composition, the inferred mantle component (extrapolated to a hypothetical parental melt with 10 wt% MgO) is likely to have had a slightly more radiogenic composition, i.e. ϵ Nd of -2. If this is also valid for the syenites from outside the shear zone, the mantle source of these rocks must have had very unradiogenic ϵ Nd values of ca. -13 because during AFC processes ϵ Nd becomes more radiogenic. Such enriched isotopic compositions are rarely observed although the initial ϵ Nd values for igneous alkaline rocks from Bunger Hills, David Island and Gaussberg have such unradiogenic isotopic compositions with initial ϵ Nd ranging from -13 to -19 (Sheraton et al. 1990, 1992). Such different isotopic compositions are most likely due to differences in the time of mantle enrichment. In the case of the syenites from outside the shear zone mantle enrichment must have occurred during the late Archaean or early Proterozoic, contemporaneous with crust formation in this area (Seth et al. 1998) whereas for the syenites from within the shear zone, the less negative ϵ Nd values for an inferred parental magma is probably due to a much younger crust formation and mantle enrichment event in this area (middle Proterozoic or early Palaeozoic).

None of the simple, single-stage models (partial melting of metasomatized upper mantle or differentiation of an alkali basaltic magma) can account for the complex geochemical and isotopic composition of the Otjimbingwe syenites. In the genesis of these syenites, the following processes were involved: (1) partial melting of a phlogopite-bearing metasomatized lithospheric mantle to produce the ne-normative parental melt. Mixing of melts from garnet-bearing and garnet-free lithologies were likely at this stage, (2) mixing of the ne-normative parental melt with qtz-normative melts from either felsic lower crust (syenites from within the shear zone) or yet another evolved melt from a distinct mantle source (syenites from outside the shear zone) to produce the qtz-normative syenites, (3) emplacement of discrete magma batches into lower crustal rocks and subsequent (4) crystal fractionation processes within each magma batch to produce the individual samples.

Acknowledgements The analytical work was supported by grants from the Max-Planck-Society and A.W. Hofmann is thanked for hospitality and free access to mass spectrometry facilities while S. J. held a post-doc position in Mainz. Iris Bambach (Max-Planck-Institut, Mainz) did a superb job in managing the line drawings. Special thanks go to D. Dohle from the Bonn fluorine-lab crew for determination of the oxygen isotope ratios. S. Göbeler (Marburg) helped with Fe^{2+} and REE determinations. E. Hoffer (Marburg) is thanked for logistic help in the field in 1998 and for free access to samples originally collected by members of the SFB 48 at the University of Göttingen. We would like to thank T. Green for making his unpublished phlogopite and amphibole trace element analyses available in 1998. CMP reviewers, two of them anonymous, as well as R. Trumbull and M. Okrusch made numerous comments which helped to clarify various aspects of the original manuscript. The patient editorial handling by J. Hoefs is gratefully acknowledged.

References

Adam J, Green TH, Sie SH (1993) Proton microprobe determined partitioning of Rb, Sr, Ba, Y, Zr, Nb, and Ta between experimentally produced amphiboles and silicate melts with variable F contents. Chem Geol 109:29–49

Boynton WV (1984) Geochemistry of rare earth elements: Meterorite studies. In: Henderson P (ed) Rare earth element geochemistry. Elsevier, New York, pp 63–114

Brotzu P, Gomes CB, Melluso L, Morbidelli L, Morra V, Ruberti E (1997) Petrogenesis of coexisting SiO_2-undersaturated to SiO_2-oversaturated felsic igneous rocks: the alkaline complex of Itatiaia, Southeastern Brazil. Lithos 40:133–156

Brown PE, Becker SM (1986) Fractionation, hybridisation, and magma mixing in the Kialineq centre, East Greenland. Contrib Mineral Petrol 92:57–70

Bühn B, Okrusch M, Woermann E, Lehnert K, Hoernes S (1995) Metamorphic evolution of Neoproterozoic manganese formations and their country rocks at Otjosondu, Namibia. J Petrol 36:463–496

Cameron AE, Smith DH, Walker RL (1969) Mass spectrometry of nanogram-size samples of lead. Anal Chem 41:525–526

Clayton RN, Mayeda TD (1963) The use of bromine pentaflouride in the extraction of oxygen from oxides and silicates for isotope analysis. Geochim Cosmochim Acta 27:43–52

Dawson JB (1987) The kimberlite clan: relationship with olivine and leucitite lamproites, and inferences for upper mantle metasomatism. In: Fitton JG, Upton BG (eds) Alkaline igneous rocks. Geol Soc Spec Publ 30:95–101

Deer WA, Howie RA, Zussman J (1992) An introduction to the rock-forming minerals. Longman Scientific, Essex

DePaolo DJ (1981) Trace element and isotopic effects of combined wallrock assimilation and fractional crystallization. Earth Planet Sci Lett 53:189–202

Erlank AJ, Waters FG, Hawkesworth CJ, Haggerty SE, Allsopp HL, Rickard RS, Menzies M (1987) Evidence for mantle metasomatism in peridotite nodules from the Kimberley pipes, South Africa. In: Menzies M, Hawkesworth CJ (eds) Mantle metasomatism. Academic, London, pp 221–311

Ewart A (1982) Petrogenesis of the tertiary anorogenic volcanic series of Southern Queensland, Australia, in the light of trace element geochemistry and O, Sr, and Pb isotopes. J Petrol 23:344–382

Fitton JG (1987) The Cameroon line, West Africa: a comparison between oceanic and continental alkaline volcanism. In: Fitton JG, Upton BG (eds) Alkaline igneous rocks. Geol Soc Spec Publ 30:273–291

Fitton JG, Upton BG (1987) Alkaline igneous rocks. Geol Soc Spec Publ 30:568

Foland KA, Landoll JD, Henderson CMB, Jiangfeng C (1993) Formation of cogenetic quartz and nepheline syenites. Geochim Cosmochim Acta 57:697–704

Foley SF (1992) Vein-plus-wallrock melting mechanisms in the lithosphere and the origin of potassic alkaline magmas. Lithos 28:435–453

Foley SF, Wheller GE (1990) Parallels in the origin of the geochemical signatures of island arc volcanics and continental potassic igneous rocks: the role of residual titanates. Chem Geol 85:1–18

Foley SF, Venturelli G, Green DH, Toscani L (1987) The ultrapotassic rocks: characteristics, classification, and constraints for petrogenetic models. Earth Sci Rev 24:81–134

Fowler MB (1992) Elemental and O-Sr-Nd isotope geochemistry of the Glen Dessary syenite, NW Scotland. J Geol Soc Lond 149:209–220

Gleason JD, Miller CV, Wooden JL, Bennett VC (1994) Petrogenesis of the highly potassic 1.42 Ga Barrel Spring pluton, southeastern California, with implications for mid-Proterozoic magma genesis in the southwestern USA. Contrib Mineral Petrol 118:182–197

Haack U, Gohn E, Klein JA (1980) Rb/Sr ages of granitic rocks along the middle reaches of the Omaruru River and the timing of orogenetic events in the Damara belt (Namibia). Contrib Mineral Petrol 74:349–360

Haack U, Hoefs J, Gohn E (1982) Constraints on the origin of Damaran granites by Rb/Sr and $\delta^{18}O$ data. Contrib Mineral Petrol 79:279–289

Haack U, Gohn E, Brandt R, Feldmann H (1988) Rb-Sr data on the Otjimbingwe Alkali complex in the Damara orogen, South West Africa, Namibia. Chemie der Erde 48:131–140

Harris NBW, Duyverman HJ, Almond DC (1983) The trace element and isotope geochemistry of the sabaloka igneous complex, Sudan. J Geol Soc Lond 140:245–256

Hartmann O, Hoffer E, Haack U (1983) Regional metamorphism in the Damara orogen: interaction of crustal motion and heat transfer. Spec Publ Geol Soc S Afr 11:233–241

Hawkesworth CJ, Fraser KJ, Rogers NW (1985) Kimberlites and lamproites: extreme products of mantle enrichment processes. Geol Soc S Afr Trans 88:439–447

Hawkesworth CJ, Kempton PD, Rogers NW, Ellam RM, van Calstern PW (1990) Continental mantle lithosphere and shallow level enrichment processes in the earth's mantle. Earth Planet Sci Lett 96:256–268

Heinrichs H, Herrmann AG (1990) Praktikum der Analytischen Geochemie. Springer, Berlin Heidelberg New York

Ionov DA, Hofmann AW (1995) Nb-Ta-rich mantle amphiboles and micas: implications for subduction-related metasomatic trace element fractionation. Earth Planet Sci Lett 131:341–356

Irving AJ, Frey FA (1984) Trace element abundances in megacrysts and their host basalts: constraints on partition coefficients and megacryst genesis. Geochim Cosmochim Acta 48:1201–1221

Jacobsen SB, Wasserburg GJ (1980) Sm-Nd isotopic evolution of chondrites. Earth Planet Sci Lett 50:139–155

Jung S, Mezger K (2001) Geochronology in migmatites: a Sm-Nd, U-Pb and Rb-Sr study from the Proterozoic Damara belt (Namibia) and implications for polyphase development of migmatites in high-grade terranes. J Metamorph Geol 19:77–97

Jung S, Mezger K (2003) Petrology of basement-dominated terranes: I. Regional metamorphic T-t path from U-Pb monazite and Sm-Nd garnet chronology (Central Damara orogen, Namibia). Chem Geol 198:223–247

Jung S, Mezger K, Masberg P, Hoffer E, Hoernes S (1998a) Petrology of an intrusion-related high-grade migmatite: implications for partial melting of metasedimentary rocks and leucosome-forming processes. J Metamorph Geol 16:425–445

Jung S, Mezger K, Hoernes S (1998b) Petrology and geochemistry of post-collisional metaluminous A-type granites: a major and trace element and Nd-Sr-Pb-O-isotope study from the Proterozoic Damara Belt, Namibia. Lithos 45:147–175

Jung S, Hoernes S, Mezger K (2001) Trace element and isotopic (Sr, Nd, Pb, O) arguments for a mid- crustal origin of Pan-African garnet-bearing S-type granites from the Damara orogen (Namibia). Precambrian Res 110:325–355

Jung S, Mezger K, Hoernes S (2002) Synorogenic melting of mafic lower crust: constraints from geochronology, petrology and Sr, Nd, Pb, O isotope geochemistry of quartz diorites (Damara orogen, Namibia). Contrib Mineral Petrol 143:551–566

Jung S, Hoernes S, Mezger K (2003) Petrology of basement-dominated terranes: II. Contrasting isotopic (Sr, Nd, Pb, and O) signatures of basement-derived granites and constraints on the source region of granite (Damara orogen, Namibia). Chem Geol 199:1–28

Lechler PJ, Desilets MO (1987) A review of the use of loss on ignition as a measurement of total volatiles in whole rock analysis. Chem Geol 63:341–344

Litvinovsky BA, Jahn BM, Zanvilevich AN, Shadaev MG (2002) Crystal fractionation in the petrogenesis of an alkali monzodiorite-syenite series: the Oshurkovo plutonic sheeted complex, Transbaikalia, Russia. Lithos 64:97–130

Lubala RT, Frick C, Roders JH, Walraven F (1994) Petrogenesis of syenites and granites in the schiel alkaline complex, Northern Transvaal, South Africa. J Geol 102:307–316

Ludwig KR (1991a) PBDAT: a computer program for processing Pb-U-Th isotope data. Version 2.75. US Geol Surv Open File Rep 88–542

Ludwig KR (1991b) ISOPLOT: a plotting and regression program for radiogenic isotope data. Version 2.75. US Geol Surv Open File Rep 91–445

Masberg HP, Hoffer E, Hoernes S (1992) Microfabrics indicating granulite-facies metamorphism in the low-pressure central Damara orogen, Namibia. Precambrian Res 55:243–257

Mattinson JM (1986) Geochronology of high-pressure-low temperature Franciscan metabasites. A new approach using the U-Pb system. Geol Soc Am Mem 164:95–105

McDermott F, Harris NBW, Hawkesworth CJ (1996) Geochemical constraints on crustal anatexis: a case study from the Pan-African granitoids of Namibia. Contrib Mineral Petrol 123:406–423

McDonough WF, McCulloch MT, Sun SS (1985) Isotopic and geochemical systematics in Tertiary-Recent basalts from southestern Australia and implications for the evolution of the sub-continental lithosphere. Geochim Cosmochim Acta 49:2051–2067

McKenzie D, O'Nions RK (1991) Partial melt distributions from inversion of rare earth elements. J Petrol 32:1021–1091

Menzies M (1987) Alkaline rocks and their inclusions: a window on the earth's interior. In: Fitton JG, Upton BG (eds) Alkaline igneous rocks. Geol Soc Spec Publ 30:15–27

Michard A, Guriet P, Soudant M, Albarède F (1985) Nd isotopes in French phanerozoic shales: external vs. internal aspects of crustal evolution. Geochim Cosmochim Acta 49:601–610

Miller R McG (1983) The Pan-African Damara orogen of South West Africa/Namibia: Spec Publ Geol Soc S Afr 11:431–515

Miller C, Schuster R, Klözli U, Frank W, Purtscheller F (1999) Post-collisional potassic and ultrapotassic magmatism in SW Tibet: geochemical and Sr-Nd-Pb-O isotopic constraints for mantle source characteristics and petrogenesis. J Petrol 40:1399–1424

Mingram B, Trumbull RB, Littman S, Gerstenberger H (2000) A petrogenetic study of anorogenic felsic magmatism in the Cretaceous Paresis ring complex, Namibia: evidence for mixing of crust and mantle-derived components. Lithos 54:1–22

Nelson DR, McCulloch MT (1989) Enriched mantle components and mantle recycling of sediments. In: Ross J (ed) Kimberlites and related rocks: their composition, occurrence, origin and emplacement. Geol Soc Aust Spec Publ 14:560–570

Nelson DR, McCulloch MT, Sun SS (1986) The origin of ultrapotassic rocks as inferred from Sr, Nd, and Pb isotopes. Geochim Cosmochim Acta 50:231–245

O'Reilly SY, Griffin WL, Ryan CG (1991) Residence of trace elements in metasomatized spinel lherzolite xenoliths: a proton-microprobe study. Contrib Mineral Petrol 109:98–113

Patchett PJ (1992) Isotopic studies of Proterozoic crustal growth and evolution. In: Condie KC (ed) Proterozoic crustal evolution. Elsevier, New York, pp 481–508

Pupin JP (1980) Zircon and granite petrology. Contrib Mineral Petrol 73:207–220

Reiners PW, Nelson BK, Ghiorso MS (1995) Assimilation of felsic crust by basaltic magma: thermal limits and extents of crustal contamination of mantle-derived magmas. Geology 23:563–566

Rogers NW, Hawkesworth CJ, Parker RJ, Marsh JS (1985) The geochemistry of potassic lavas from Vulsini, central Italy and implications for mantle enrichment processes beneath the Roman region. Contrib Mineral Petrol 90:244–257

Sawyer EW (1981) Damaran structural and metamorphic geology of an area southeast of Walvis Bay, SW Africa/Namibia. Mem Geol Surv SW Africa/Namibia 7:1–94

Seth B, Kröner A, Mezger K, Nemchin AA, Pidgeon RT, Okrusch M (1998) Archaean to Neoproterozoic magmatic events in the Kaoko belt of NW Namibia and their geodynamic significance. Precambrian Res 92:341–363

Seth B, Jung S, Hoernes S (2002) Isotope constraints on the origin of Pan-African granitoid rocks in the Kaoko Belt, NW Namibia. S Afr J Geol 105:179–192

Sheraton JW, Black LP, McCulloch MT, Oliver RL (1990) Age and origin of a compositionally varied mafic dyke swarm in the Bunger Hills, East Antartica. Chem Geol 85:215–246

Sheraton JW, Black LP, Tindle AG (1992) Petrogenesis of plutonic rocks in a Proterozoic granulite-facies terrane—the Bunger Hills, East Antartica. Chem Geol 97:163–198

Smith IEM, White AJR, Cappell BW, Eggleton RA (1988) Fractionation in a zoned monzonite pluton: Mount Dromedary, southeastern Australia. Geol Mag 125:273–284

Smith DR, Barnes C, Shannon W, Roback R, James E (1997) Petrogenesis of mid-Proterozoic granitic magmas: examples from central and western Texas. Precambrian Res 85:53–79

Stacey JS, Kramers JD (1975) Approximation of terrestrial lead isotope evolution by a two-stage model. Earth Planet Sci Lett 26:207–221

Sutcliff RH, Smith AR, Doherty W, Barnett RL (1990) Mantle derivation of Archaean amphibole-bearing granitoids and associated mafic rocks: evidence from the Southern Superior Province, Canada. Contrib Mineral Petrol 105:255–274

Thirlwall MF, Burnard P (1990) Pb-Sr-Nd isotope and chemical study of the origin of undersaturated and oversaturated shoshonitic magmas from the Borralan pluton, Assynt, NW Scotland. J Geol Soc Lond 147:259–269

Thirlwall MF, Upton BGJ, Jenkins C (1994) Interaction between continental lithosphere and Iceland plume: Sr-Nd-Pb-isotope geochemistry of Tertiary basalts. J Petrol 35:839–879

Woolley AR, Jones GC (1987) The petrochemistry of the northern part of the Chilwa alkaline province, Malawi. In: Fitton JG, Upton BG (eds) Alkaline igneous rocks. Geol Soc Spec Publ 30:335–355

Zanvilevich AN, Litvinovsky BA, Wickham SM, Bea F (1995) Genesis of alkaline and peralkaline syenite-granite series, the Khartonovo pluton (Transbaikalia, Russia). J Geol 103:127–145

Zhao JX, Shiraishi K, Ellis DJ, Sheraton JW (1995) Geochemical and isotopic studies of syenites from the Yamato Mountains, East Antartic: implications for the origin of syenitic magmas. Geochim Cosmochim Acta 59:1363–1382